Final Scientific/Technical Report-EMSP 86981

Reporting Period:September 15, 2002 through September 14, 2006

Submission Date: December 27, 2006

Agreement Number: DE-FG07-02ER63507

Project Title: **Transport, Targeting, and Applications of Metallic Functional Nanoparticles for Degradation of DNAPL Chlorinated Organic solvents**

Investigators: **Gregory V. Lowry[1,3] (PI)**
Sara Majetich[4] (Co-PI)
Krzysztof Matyjaszewski[2] (Co-PI)
David Sholl[3] (Co-PI)
Robert Tilton[3] (Co-PI)

Carnegie Mellon University, Pittsburgh, PA
[1]Department of Civil and Environmental Engineering, [2]Chemistry,
[3]Department of Chemical Engineering, [4]Physics

Researchers: **Dr. Abdulwahab Almusallam, Dr. Bruno Dufour, Yueqiang Liu, Dr. Jeongbin Ok, Tanapon Phenrat, Navid Saleh, Dr. Traian Sarbu, Kevin Sirk, Hye-Jin Kim**

Contact: **Gregory V. Lowry, 412-268-2948, glowry@cmu.edu**

Executive Summary:

Dense Non-Aqueous Phase Liquid (DNAPL) such as trichloroethylene act as long term sources of groundwater contaminants and are difficult and expensive to remediate. DNAPL-contaminated sites are a significant financial liability for the Department of Energy and the private sector. The objective of this study was to engineer reactive Fe^0-based nanoparticles with specialized polymeric coatings to make them mobile in the subsurface and to provide them with an affinity for the DNAPL/water interface. The synthesis, characterization, and reactivity/mobility of the engineered particles, and a molecular dynamic model that predicts their behavior at the DNPAL/water interface are described in this report.

The reactive core of the particles is a Fe^0/Fe-oxide core shell particle. Two types of particles were fully characterized to determine the particle properties most desirable for in situ remediation in terms of reactivity and lifetime. The two nanoscale zerovalent iron (NZVI) particles evaluated were quite different in terms of reactivity with TCE and reactive lifetime. NZVI made for the borohydride reduction process (Fe/B) had primary particles from 25 to 40 nm in diameter that were amorphous and contained up to 20 atom % boron in the particles. Their amorphous nature enabled them to active and use H_2 for TCE reduction. A second type of NZVI evaluated (RNIP) also have primary particle sizes of 40 to 60 nm, but were crystalline and could not activate and use H_2 for TCE reduction. Both types of NZVI aggregated in water to form fractal aggregates of particles with hydrodynamic diameters between 20 to 70 micrometers in <30 minutes. The rapid aggregation was due to the magnetic attractive forces between the particles. The rate of aggregation and the final aggregate size depended on the initial concentration of the particles in the slurry and their saturation magnetization. This rapid aggregation to micron-sized aggregates, and subsequent sedimentation from suspension necessitated the use of surface modifiers to maintain stable suspensions of nanosized particles that could be transported through water-saturated porous media.

Physisorption of amphiphilic triblock copolymers synthesized by Atom Transfer Radical Polymerization (ATRP) and with the general structure poly(methacrylic acid)]-[poly(alkyl methacrylate)]-[poly(styrene sulfonate)] enhanced the stability and mobility of NZVI suspensions through porous media, and provided the particles an affinity for the DNAPL/water interface. The mass of polymer physisorbed to NZVI ranged from 1 to 4 mg/m^2 of particle surface area. Increasing the solution ionic strength increased the sorbed mass of polymer. The solution pH did not affect polymer sorption to the particles. The type and degree of polymerization of each block affected the sorbed mass, indicating that polymer architecture influenced their sorption properties. Once adsorbed, polymer desorption was negligible for up to 12 weeks.

The triblock copolymer modified nanoiron ranged in size from 100 to 200 nm as determined by dynamic light scattering. The triblock copolymer coating increased the dispersion stability, enabling ~50% of the particles to remain suspended for weeks to months. The stability enhancement was increased by increasing the polystyrene sulfonate block degree of polymerization. The triblock copolymer coatings provided the NZVI an affinity for the NAPL/water interface, as evidenced by the ability of the coated particles to emulsify TCE whereas uncoated particles could not. Brownian dynamic models were developed to predict the behavior of polymer coated particles at the DNAPL/water interface. These models indicate that the polymer architecture, in terms

of block type and degree of polymerization can be tuned to achieve specific targeting affinity.

There were notable differences in the reactivity with TCE between the types of NZVI evaluated. NZVI made from the borohydride reduction method had higher TCE dechlorination rates and yielded primarily the saturated reaction product ethane, where RNIP made from a different process had slower (but still rapid) dechlorination rates and yielded primarily unsaturated reaction intermediates (acetylene) and products ethane. The less saturated products formed by RNIP indicate the potential for a higher yield, i.e. TCE dechlorinated per mass of NZVI, as reduction to acetylene and ethene requires fewer electron than reduction to ethane.

TCE reduction and H_2 evolution (reduction of H^+) are competing processes. H_2 evolution was first order with respect to $[H^+]$ and the Fe^0 content of the particles, whereas TCE reduction was found to be aero order with respect to the Fe^0 content of the particles and ~0.16 order with respect to $[H^+]$. This indicates that H_2 evolution will be rapid initially and slow over time, whereas the TCE reduction rate will remain stable over the lifetime of the particle. H_2 evolution was inhibited at TCE concentrations greater than 1.3 mM and more of the Fe^0 was used to reduce TCE compared to application at TCE concentration less than 1.3 mM. The reactive lifetime was only a few weeks at high TCE (oxidant) loadings compared to several months at low TCE concentration. The reactive lifetime of NZVI ranged from a few weeks at near neutral pH (6.5 to 7.5) and up to a year at pH≥8. Groundwater dissolved solutes (5 mM) decreased the TCE reduction rate by up to a factor of 7, increasing in the order Cl^-, SO_4^{2-}, HCO_3^-, $H_2PO_4^-$, but had no effect on H_2 evolution. Polymer modification of RNIP decreased its reactivity with TCE by up to a factor of 10, depending on the molecular weight of the polymer used. These data indicate that NZVI reactivity with TCE should not be affected significantly by constituents in groundwater, however the site geochemistry (particularly pH) and oxidant loading are important considerations for predicting the reactive lifetime of the particles in field application. The use of NZVI in DNAPL source zones where TCE concentrations are high will increase the efficiency of Fe^0 utilization. Polymer modification is necessary for mobility of the particles, however, so there will be a tradeoff between mobility and reactivity as these modifiers lower the reactivity of the particles.

Surface modification of NZVI is essential to enhancing their mobility in water saturated porous media. Under normal groundwater conditions of ionic strength and ionic composition, the mobility of bare particles at 3 g/L is only a few centimeters whereas the mobility of polymer modified particles is 10's to 100's of meters. The primary mode of filtration at high particle concentrations (3 g/L) is physical straining. At low particle concentration (30 mg/L) the primary mode of filtration is attachment to the media grains. Mobility enhancement is a function of the modifier type and of the groundwater geochemistry, in particular the ionic strength and presence of divalent cations Ca^{2+} or Mg^{2+}. Low molecular weight surface modifiers that rely on electrostatic repulsions for enhanced mobility are affected by changes in groundwater geochemistry, while high molecular weight surface modifiers that afford electrosteric repulsions are not and can be effective at high salt concentrations. Given that different modifiers respond differently to changes in ionic strength and composition, it is possible to tailor the properties of the surface modifier to the groundwater geochemistry in order to achieve a specified mobility, i.e. radius of influence from the injection point.

1.0 Project Goals and Objectives

This project addressed the need for methods to remove or degrade subsurface contaminants that are present as dense non-aqueous phase liquids (DNAPLs) and act as long-term sources of groundwater contamination. The goal was to build on a particle-based approach to subsurface contaminant remediation that is based partly on the recent success in using nanoiron to degrade chlorinated compounds dissolved in groundwater, and knowledge of how colloids migrate in porous media. The specific project objective was to engineer reactive Fe^0-based nanoparticles with specific coatings to make them mobile in the subsurface and to provide them with an affinity for the DNAPL/water interface. At the interface, the particles decompose DNAPL pollutants to non-toxic products. Delivering reactive particles directly to the surface of the DNAPL will decompose the pollutant into benign materials, reduce the migration of pollutant during treatment, and reduce the time needed to remove residual pollution by other means, such as natural attenuation.

Contributions from several basic science fields were used to advance a particle-based strategy for *in situ* DNAPL degradation by providing targeted delivery of reactive particles directly to the DNAPL. Specific project elements included the following.

1. **Particle synthesis and characterization**. Synthesized reactive Fe^0 particles that rapidly and efficiently dechlorinated TCE to harmless products.
2. **Particle surface modification.** Amphiphilic block copolymers were synthesized using ATRP and characterized, and the polymers were physisorbed to the particle surfaces.
3. **Polymer-coated particle characterization.** The physical and chemical properties of the polymer-coated particles were characterized, including their NAPL targeting ability.
4. **Particle reactivity analysis.** The efficacy and efficiency of Fe^0 nanoparticles synthesized by different methods were determined. The effect of water quality parameters and the adsorbed polymer coatings on the reactivity and efficiency were determined.
5. **Particle mobility.** The mobility and in situ water-DNAPL partitioning of particles in saturated porous media was determined using micro-model and intermediate scale experiments in porous media. The effect of how physical, chemical, and hydrologic regimes existing in the subsurface affected nanoparticle migration was also determined.
6. **Particle-level computer model.** A predictive numerical model for the transport and DNAPL partitioning of surface modified nanoparticles in bench-scale and meso-scale experiments was developed.

2.0 Project Accomplishments

The following describes the results obtained relating to each project objective and the implications of those results on the applicability of the nanoparticle-based remediation strategy for subsurface DNAPL source zones.

2.1. Particle synthesis and characterization.

Particle properties. Two types of unmodified iron nanoparticles were investigated, Reactive Nanoscale Iron Particles (RNIP, supplied by Toda American, Inc.) and Fe^0 nanoparticles (Fe/B) synthesized in our laboratory using a slightly modified aqueous sodium borohydride reduction method previously reported Zhang, 2003; Liu et al, 2005a). RNIP particles are synthesized commercially by reduction of Fe-oxides in H_2 gas followed by controlled exposure to water to generate a Fe^0/Fe_3O_4 (core/shell), and available in large quantities. To investigate the effects of structure (amorphous vs. crystalline) on the reactivity, one derivative of FeB, FeB^{cr}, was obtained by annealing FeB at 400°C for 3 hours under pure H_2.

The iron particle sizes, morphology, and chemical information were determined by TEM/SAED, XRD, XPS, and N2-BET. A summary of the characterization of the particles is shown in Table 1 (Liu et al., 2005b).

Table 1. Summary of characterization of the nanoscale iron particles

	FeB	FeB^{cr}	RNIP
Size	25-40nm	25-40nm	40-60nm
SA	33.7m^2/g	16.9m^2/g	23m^2/g
Shell thickness	5-6	2.5-4	5-10
Shell composition	B: 5% Fe: 17% O: 53%	B: 23% Fe: 4% O: 50%	Fe: 26% O: 52-54%
Crystallinity	amorphous	crystalline	crystalline
Fe^0 content	86%	89%	27-70%
B content	5.2%	5.1%	0%

TEM (Figure 1) and BET show that size (25-60nm) and specific surface area (17-34m^2/g) are similar among the nanoscale particles investigated, and similar to others reported in the literature (Nurmi et al., 2005). The initial Fe^0 content measured using 1M HCl digestion is ~90% for fresh FeB and 27-70% for RNIP. The large range in Fe^0 content was due to the age of the particles as the half life time for Fe^0 in the particles was approximately 3 months (Liu and Lowry, 2006). The HRTEM indicated a core/shell morphology of all the RNIP, FeB, and FeB^{cr} particles. XRD demonstrated the amorphous structure of FeB whereas FeB^{cr} and RNIP were crystalline (Figure 2). SAED (or ED) of the particles confirmed the crystalline degree in each type of the particles. As discussed below, the reactivity of the particles, and the ability of the particles to activate

and use $H_{2(aq)}$ was a function of the crystallinity of the particles. The amorphous FeB was able to activate and use H_2 whereas the crystalline forms of Fe^0 were unable to. The degree of crystallinity also affected the reactive lifetime of the particles, with the crystalline particles being more resistant to rapid oxidation that the amorphous FeB particles.

Both particles synthesis methods produce Fe^0 nanoparticles with similar sizes, surface areas, and reactivity with trichloroethylene (TCE). However, the low cost and commercial availability of RNIP makes it an attractive Fe^0 particle for use in field applications. Because of this, RNIP particles were used in all of the follow on work relating to mobility and DNAPL targeting.

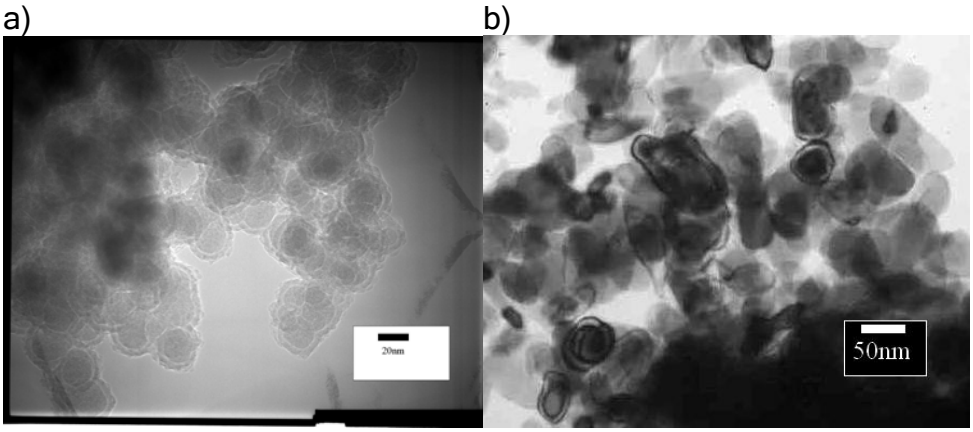

Figure 1. TEM images of fresh particles; a) Fe/B and b) RNIP

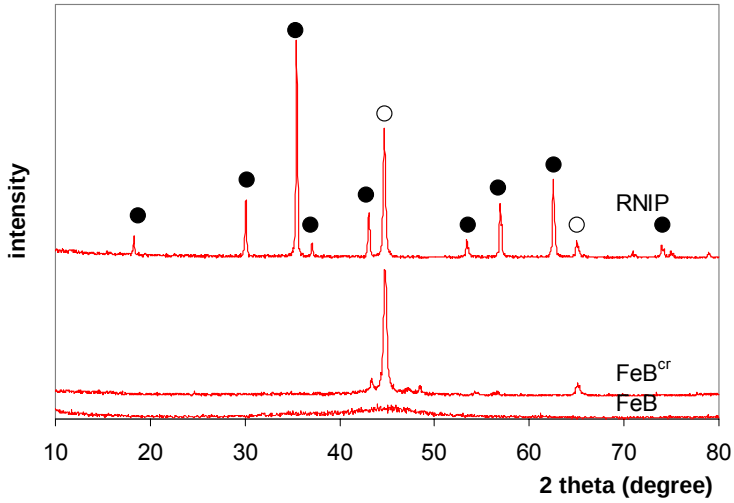

Figure 2. XRD pattern of FeB, FeB^{cr} and RNIP, ●: Fe3O4, ○: Fe^0

Properties of aqueous suspensions of bare RNIP. Bare RNIP was characterized for its Fe^0 content, magnetic properties, zeta potential (Phenrat et al., 2006). These parameters govern particle-particle interaction and influence RNIP mobility in water-saturated porous media. According to the remnant magnetization (M_r), saturation magnetization (M_s), and coercivity (H_c), obtained from the hysteresis cycle of the magnetization loop using SQUID, the ratio of M_r/M_s for RNIP is 0.13 while its H_c is 12.6 mT. Based on these magnetic parameters, RNIP is classified as pseudo-single domain ($0.1<M_r/M_s<0.5$ and $10<H_c<15$ mT). For RNIP with Fe^0 content of 14.3% and 26%, the M_s is 570 and 741 kA/M, respectively. The zeta potentials of RNIP with 14.3 and 26% Fe^0 are -31.7 mV (pH=7.5) and -38.8 (pH=8.5) in 1mM $NaHCO_3$ and 1mM NaCl. Extended DLVO theory which takes into account the long-range magnetic attractive and van der Waals (Hamaker constant of RNIP = 10^{-19}) forces against electrostatic repulsion, attraction overcomes repulsion for these particles and no energy barrier to aggregation exists. Thus, rapid aggregation is predicted. This is in good agreement with experimental results using Dynamic Light Scattering (DLS) and Optical Microscopy which showed rapid aggregation of RNIP from single nanoparticles to micron size aggregates and further to inter-connected fractal aggregates. The rate of aggregation was a function of the particle concentration and the saturation magnetization of the particles (Figure 3). For RNIP with 14.3% Fe^0 primary particles (average radius = 20 nm) aggregate to micron-size aggregates in only 10 minutes, with average hydrodynamic radii ranging from 125 nm to 1.2 μm at a particle concentration of 2 (volume fraction($\varnothing$=3.2 x10^{-7}) and 60 mg/L ($\varnothing$ =9.5 x10^{-6}), respectively. It should be noted that the number-averaged particle size distribution of bare RNIP also changes significantly as a function of time indicating that the majority of the bare RNIP population rapidly aggregates. Subsequently, these aggregates assemble themselves into fractal, chain-like clusters. At an initial concentration of just 60 mg/L and ionic strength or 1 mM, cluster sizes reach 20 to 70 μm in 30 minutes and are rapidly sedimented from solution (Phenrat et al., in press). This rapid aggregation inhibited their mobility in water saturated porous media, necessitating the use of surface coatings to make the particles mobile.

2.2. Particle surface modification.

Polymer Coatings. Fe^0 nanoparticles are essentially immobile in saturated porous media (Saleh et al., 2007; Schrick et al., 2004) and thus require surface coatings to make them mobile. These same surface coatings, if made amphiphilic, can be used to impart to the particles an affinity for the NAPL/water interface. Amphiphilic triblock copolymers were synthesized using Atom Transfer Radical Polymerization (ATRP), which is well-known as a robust technique for control/living radical polymerization (Wang and Matyjaszewski, 1995; Matyjaszewski and Wang, 1995; Patten et al., 1996; Pyun and Matyjaszewski, 2001). The resulting polymers were then adsorbed to the RNIP to create a Fe^0 core-polymer shell particle that were able to partition to the DNAPL/water interface and were highly mobile and resistant to changes in ionic strength and composition. The synthesis of polymers and characterization of the resulting polymer-modified RNIP are described here.

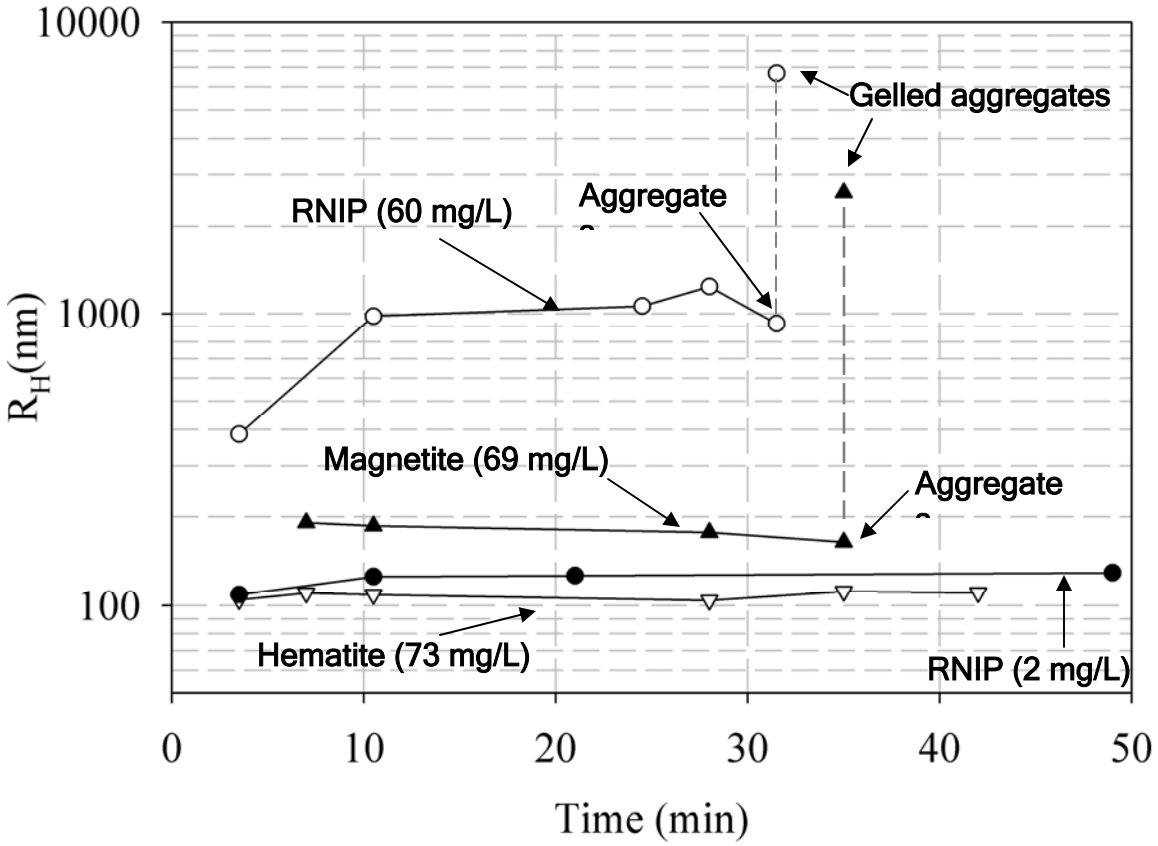

Figure 3. Evolution of average R_H of dominant size class as a function of time for RNIP (14.3% Fe^0 and M_s = 570 kA/M), magnetite (M_s = 330 kA/M), and hematite(M_s = 14 kA/M). Last measured points for RNIP and magnetite become bimodal distribution with larger size due to gelation of aggregates.

Preparation of well-defined block copolymers for the functionalization of iron nanoparticles. To improve the stability of iron nanoparticles in water media and soil, the particles were functionalized with a triblock copolymer through interaction between a poly(methacrylic acid) segment and iron. The [poly(methacrylic acid)]-[poly(alkyl methacrylate)]-[poly(styrene sulfonate)] amphiphilic block copolymer is designed to allow the reduction of chlorinated solvents by the functionalized iron nanoparticles by placing them directly at the water/DNAPL interface. Poly(methacrylic acid) (PMAA) is the anchoring block to the iron nanoparticles. Either poly(methyl methacrylate) (PMMA) or poly(butyl methacrylate) (PBMA) was used as the hydrophobic block to improve the solubility of the nanoparticles in DNAPL and to protect the iron nanoparticle from oxidation during transport in the soil. Poly(styrene sulfonate) (PStS) block was used as the hydrophilic charged segment to allow prevent aggregation and attachment of the iron nanoparticles to soil grains and organic carbon and via electrosteric repulsions. The general structure for the polymer architecture is shown in Figure 4.

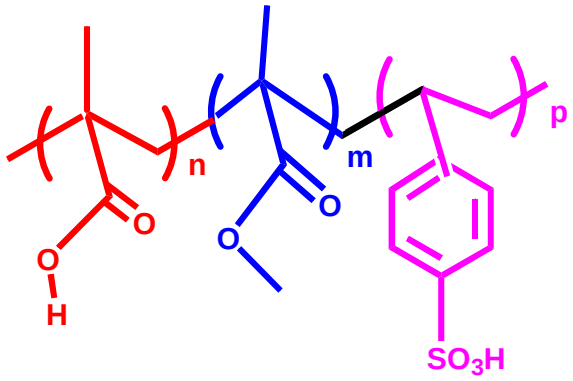

Figure 4. Hydrophobic-hydrophilic triblock copolymers containing a short anchoring group. Red-PAA anchoring block, Blue-PMMA or PBMA hydrophobic block, Pink-hydrophilic sulfonated polystyrene block.

The triblock copolymers were prepared using ATRP as described in Figure 5. ATRP has been proven to be an efficient method for the preparation of polymers and copolymers with well defined chain length and architectures. Due to the instability of the copper catalyst used in ATRP towards acidic groups, this method involves two post-functionalization reactions on a precursor polymer: sulfonation of polystyrene by acetyl sulfate to obtain a poly(styrenesulfonic) block, and hydrolysis of the ester bond of poly(tert-butyl methacrylate) to obtain the poly(methacrylic acid) anchoring block. Acetyl sulfate is known to be a quantitative sulfonation agent, provided it is used in large excess. Sulfonation degree was determined on polystyrene sulfonate using elemental analysis and was quantitative (98%). An example of evolution of GPC traces during each block extension is presented in the figure below. Clear shift of the molecular weight distribution at each step is observed, demonstrating the successful preparation of the block copolymer. Polymers with similar architecture (Figure 4), but of different compositions were successfully synthesized by ATRP, and are described in Table 2 (polymers used for functionalization of iron particles are in red). The polydispersity index (PDI) was low (below 1.6) at each step of the block copolymer synthesis, demonstrating the good control on the length of each constituting segment and architectures synthesized for this project are given in Table 2. Appropriate hydrophobic and hydrophilic polymer blocks for the intended purpose of surface modification are shown in red. These polymers were used to study mobility, NAPL targeting, and their effects on reactivity.

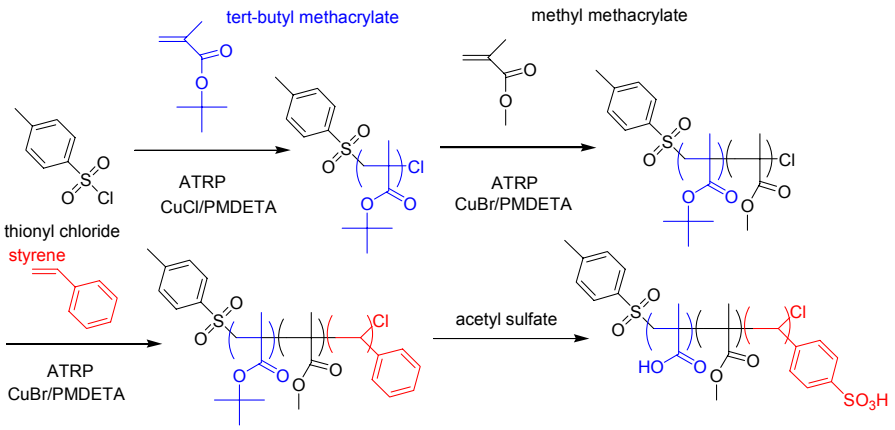

Figure 5. Preparation scheme of triblock copolymer by ATRP

Table 2. Composition and polydispersity of polymers prepared by ATRP

Composition	Mn (g/mol)	PDI
$tBMA_{15}$	2160	1.16
$tBMA_{48}$	6800	1.26
$tBMA_{48}$-MMA_{17}	8500	1.23
MAA_{48}-MMA_{17}-StS_{650}	125400	1.62
MAA_{14}-MMA_{57}-StS_{80}	24310	1.52
MAA_{15}-MMA_{64}-StS_{75}	23980	1.41
MAA_{15}-MMA_{60}-StS_{150}	39030	1.28
MAA_{43}-MMA_{26}-StS_{597}	131688	1.14
MAA_{15}-StS_{811}	169196	1.40
MAA_{15}-BMA_{43}-StS_{811}	175302	
MAA_{47}-MMA_{51}-StS_{450}	104474	
MAA_{41}-MMA_{26}-StS_{462}	103594	
MMA_{45}-StS_{609}	129954	

Particle Surface Modification. Sorption of the synthesized tri-block co-polymers to RNIP was measured by the solution depletion technique. For each isotherm, a fixed amount of iron was added to varying polymer concentrations in 1mM $NaHCO_3$ and 1mM $NaHCO_3$ + 50 mM NaCl solutions. The pH of these samples was between 7-8. The measured specific area was 4.93 m^2/g. A typical sorption isotherm at each ionic strength is shown in Figure 6.

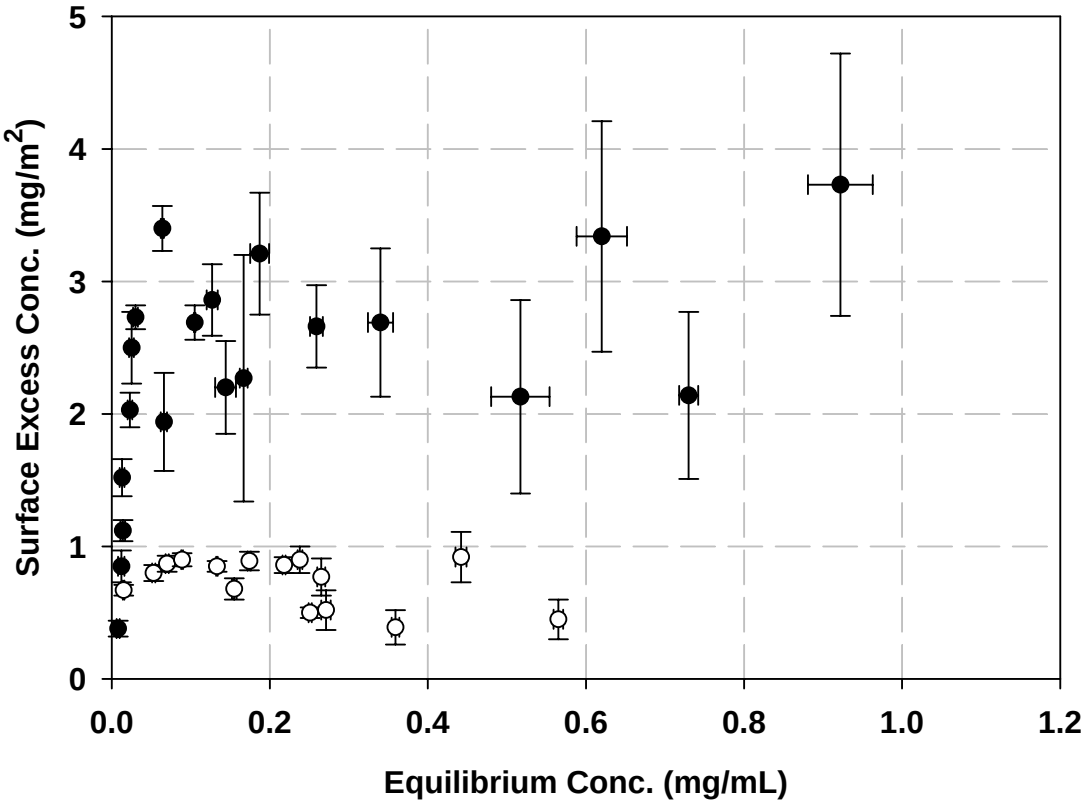

Figure 6. Adsorption isotherms of $PMAA_{15}$-PSS_{811} (○ open circles) and $PMAA_{15}$-$PBMA_{43}$-PSS_{811} (● closed circles) on RNIP. These samples were in 1 mM $NaHCO_3$ + 50 mM NaCl solutions.

Several conclusions were drawn from the polymer sorption studies (Sirk et al., submitted). First, all of the polymers synthesized adsorbed to the iron particles at concentrations of 1-3 mg/m^2. When the ionic strength of the solution was increased, the surface excess concentration for each polymer also increased. This is due to the screening of the negative charges on the polymers by the additional salt. This screening reduces the repulsions between polymers that in turn increases the number of polymers adsorbed to the iron surface. The second conclusion is that the polymer architecture does have a measurable effect on the amount adsorbed to the iron surface. The presence of a hydrophobic block (either MMA or BMA) adds an additional driving force for adsorption that increases the total surface excess concentration by a factor of 2 to 3. This is evident in Figure 6 above. Also, by removing the PMAA anchor block, adsorption decreased by a factor of ~2 compared to polymers with similar architecture but that contained the PMAA block. We have found no measurable desorption of the polymers from the particle surface indicating irreversible adsorption of these polymers.

2.3 Polymer-coated particle characterization and NAPL-water interface targeting.

Polymer-modified particle characterization. RNIP modified with two of the synthesized triblock copolymers were characterized in terms of size, surface charge, and stability (Table 3) (Saleh et al., 2005).

Table 3. Polymer Properties and Mean DLS Particle Sizes and Electrophoretic Mobility Measured in a 1 mM $NaHCO_3$ Solution (pH=7.4).

polymeric surface modification	M_n[a] (PDI[b])	mean diameter (nm)	electrophoretic mobility (μmcm/Vs)
none		146 ± 4	−2.3 ± 0.15
$PMAA_{42}$–$PMMA_{26}$–PSS_{462}	56 100 (1.24)	178 ± 11	−3.82 ± 0.16
$PMAA_{48}$–$PMMA_{17}$–PSS_{650}	75 600 (1.62)	212 ± 21	−3.14 ± 0.07

[a] Measured before sulfonation. [b] Polydispersity index.

In a 1mM $NaHCO_3$ solution and 30 mg/L, bare RNIP ranged in size from 100 to 200 nm as determined by light scattering and have a measured electrophoretic mobility of -2.3±0.15μmcm/Vs (Figure 7a). Bare RNIP has particle size varying from 100-200 nm (which is 2-10 times higher than the primary particle size). This was due to pre-existing aggregates that were unable to be separated by sonication. The particle size distribution shows the increase in particle size after modification. Modifying the particles with triblock copolymers increases their surface charge (Table 3) and, given the high molecular weight of those polymers, also provided steric repulsions that enhanced their colloidal stability (Figure 7b).

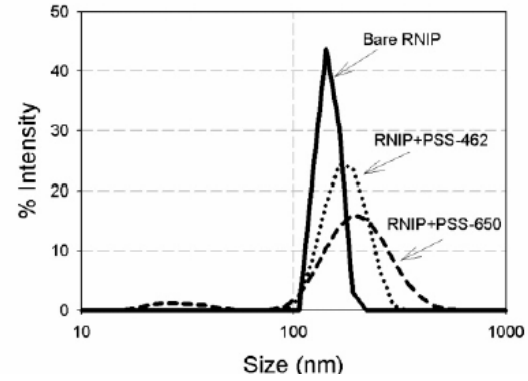

Figure 7(a). DLS intensity data for bare and modified iron nanoparticles.

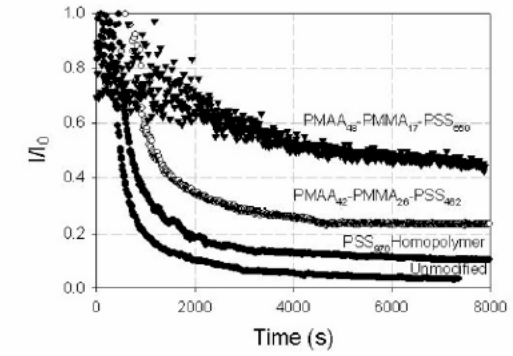

Figure 7(b). Sedimentation curves for bare and modified iron nanoparticle dispersions (0.08 wt %) in water.

Bare RNIP aggregated and rapidly sedimented from solution due to short range van der Waal's interactions and other long-range forces attributed to the magnetic properties of

Fe^0/Fe_3O_4 (Figure 7 (b)). Triblock copolymers with longer PSS chain demonstrated higher stability than the shorter PSS blocks. (Saleh et al., 2005; Phenrat et al., 2007).

NAPL-water interfacial targeting. Two types of polymer-modified particles were evaluated. First was a PSS-modified silica nanoparticle (Saleh et al., 2005b). Second was the triblock-copolymer modified RNIP (Saleh et al., 2005a). To test the targeting ability of the polymer-coated particles, we measured their influence on the interfacial tension of the TCE/water interface. Figure 8 shows that PSS-Si particles decreased the TCE/water interfacial tension appreciably. For comparison, unmodified silica particles having approximately the same radius (50 nm) as that of the PSS-Si particles had no effect on the interfacial tension, as expected. This demonstrates that the grafted PSS chains penetrated the TCE/water interface as the particles adsorbed. PSS homopolymers in aqueous solution decreased the TCE/water interfacial tension to 22.5 and 14.5 mN/m at concentrations of 1 and 5 mg/mL, respectively, confirming that PSS is surface active.

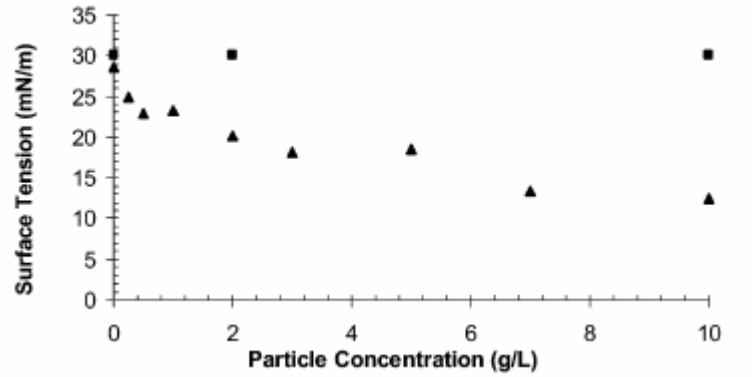

Figure 8. TCE/water interfacial tension as a function of the particle concentration in water for (■) unmodified silica particles and (▲) PSS-grafted silica particles at room temperature.

Further evidence for the interfacial targeting capabilities of the PSS-grafted particles was provided by emulsification experiments using TCE and heptane with PSS-Si particles. All emulsions formed were water continuous (based on the emulsion phase conductivity values that ranged from ~20 to 4000 μS/cm) suggesting that these particles produced non-invertible emulsions. Figures 9 (a)-(b) show representative optical micrographs of emulsions prepared with TCE and heptane. Emulsion characteristic details are described in Saleh et al., (2005b). Emulsion characterization determined that emulsion phases with greater than 6 months stability were formed using only 0.04-0.07 wt% PSS-Si. The analysis also concluded that a monolayer coverage of particles is a minimal requirement for emulsion stability in the system. The ability of these hydrophilic charged particles to function as emulsifiers was attributed to the hydrophobic character of the vinyl backbone.

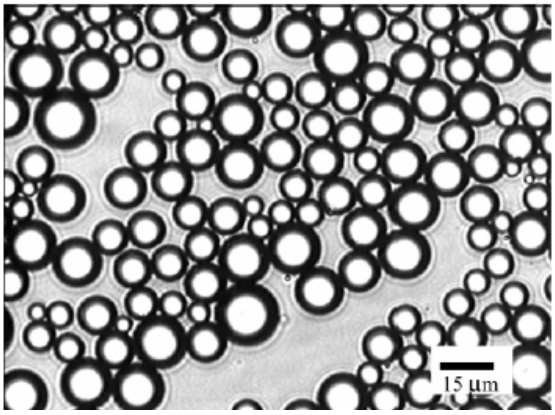

Figure 9a. Optical micrograph of the TCE/water emulsion phase sampled from a preparation containing 0.75 mg/mL of PSS-Si particles and a 2.5:7.5 TCE/water ratio. The emulsion phase is 83% (v/v) TCE.

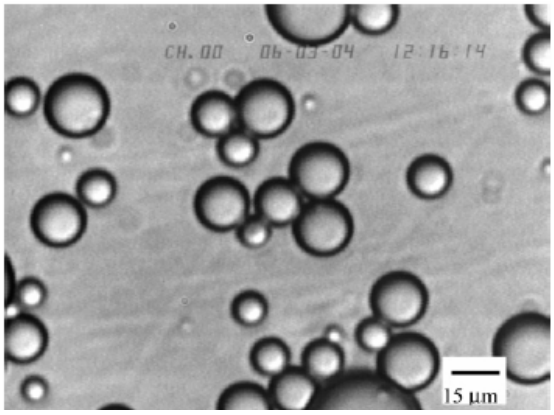

Figure 9b. Optical micrograph of the heptane/water emulsion phase sampled from a preparation containing 0.50 mg/mL of PSS-Si particles and a 1:5 heptane/water ratio.

Triblock copolymer-modified RNIP. The triblock copolymers were designed with a specific architecture that provided them with amphiphilicity so that the modified RNIP can transport in groundwater as well as localize at NAPL/water interface. Emulsification experiments were performed to demonstrate NAPL/water targetability of polymer modified RNIP. Figure 10 (a)-(d) presents representative micrograph images showing emulsion droplets stabilized with modified RNIP. Fractionated and "raw" RNIP suspensions modified with triblock copolymers successfully emulsified NAPL, demonstrating the targetability of the surface modified particle. PSS homopolymer and diblock copolymer modified RNIP were unable to emulsify any NAPL phase. This demonstrated the significance of the polymer architecture to achieve NAPL targetability. Highly controllable triblock architecture thus has the potential to optimize the transport and targeting ability of the RNIP. Optimization of the polymer architecture is continuing under a separate grant from the U.S. National Science Foundation.

2.4 Particle Reactivity

Nano sized Fe^0 particles favorable for the rapid degradation of trichloroethene (TCE), including a high surface area normalized reaction rate constant for TCE reduction at various contamination levels (part-per-million plume concentrations up to DNAPL saturation), formation of fully dechlorinated nontoxic products, high accessibility (more than 50%) of the Fe^0 in the particles, stable reactivity over the lifetime of the particles, and only minor effects of groundwater constituents on the particle reactivity. The effect of the polymer modification on particle reactivity is relatively minor, even for high the molecular weight polymers with the architecture used in this study. NZVI treatment of DNAPL source areas is preferred over their use in groundwater plumes where the contaminants are present at low concentration.

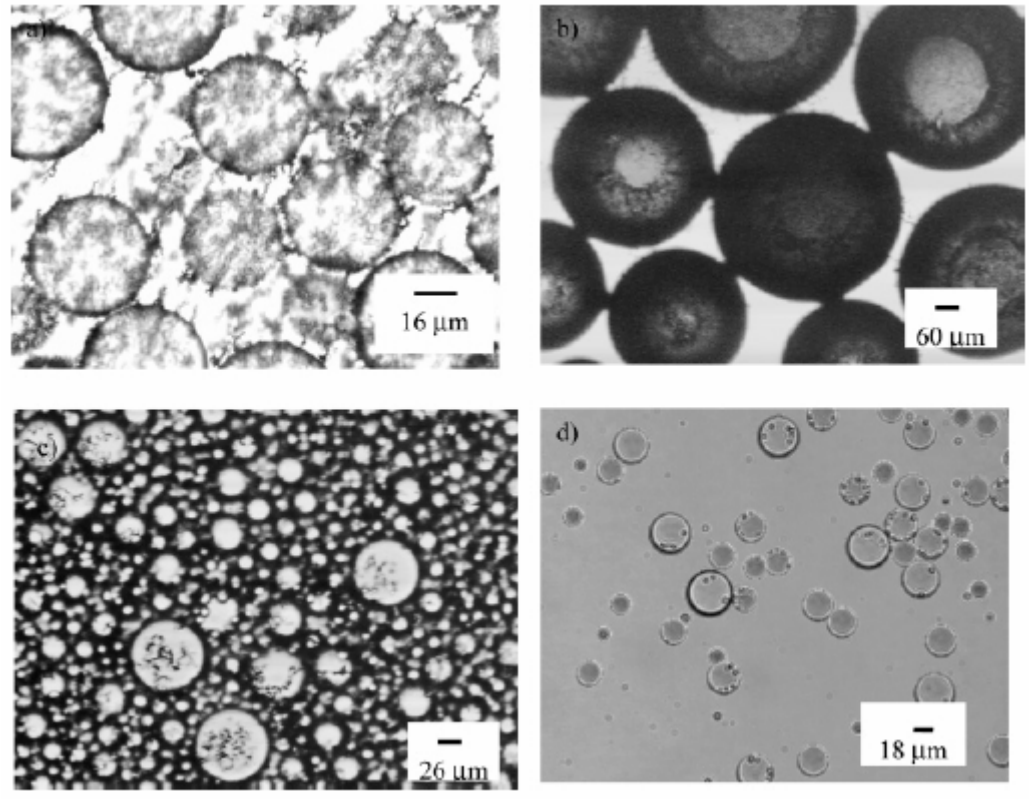

Figure 10. Micrographs of emulsified TCE (a-b) and dodecane (c) droplets in water stabilized by raw $PMAA_{42}$-$PMMA_{26}$-PSS_{462} triblock copolymer-modified iron nanoparticles and TCE (d) by fractionated $PMAA_{42}$-$PMMA_{26}$-PSS_{462} triblock copolymer-modified iron nanoparticles.

The particle reactivity is discussed below following four major sections, (a) the reactivity of nanoiron with different properties and a discussion of the particle properties of nanoiron mostly influencing their reactivity; (b) the lifetime and reactivity of RNIP; (c) the effect of groundwater constituents on the lifetime and reactivity of RNIP; and (d) the reactivity of RNIP with polymer surface modification.

Reactivity of nanoiron with different properties and a discussion of the particle properties of nanoiron mostly influencing their reactivity. The reactivity and efficiency of FeB and RNIP were compared, and the differences in their reactivity were attributed to specific particle properties (Liu et al, 2005a, 2005b). Both Fe/B and RNIP are highly reactive and rapidly transform trichloroethylene (TCE) to nontoxic compounds. The primary differences between the particle types are summarized in Table 4.

Fe/B: The reactions, which were complete in <5 days, transformed TCE to ethane. Adding H_2 increased the TCE dechlorination rate and doubled the TCE degraded, which was more than could be achieved if Fe^0 were the only reductant (Figure 11). This indicates the ability of Fe/B to activate H_2 and to use it for TCE dechlorination. Fe^0 was completely accessible and used. The concomitant and complete release of boron from

the particles suggested the oxidative dissolution of the FeB particles during their reaction with TCE.

Table 4. Differences in reactivity between FeB and RNIP.

	FeB	FeB^{cr}	RNIP
H_2 production in water	High & fast	Low & slow	Low & slow
H_2 activation	Yes	No	No
Products (main product)	Mostly saturated (ethane)	Unsaturated (acetylene)	Unsaturated (acetylene)
Fe^0 accessibility	complete	incomplete	incomplete

Using excess iron (which represents their use in a contaminant plume at low TCE concentration), Fe/B transformed TCE into ethane (80%) and C3-C6 coupling products with a surface-area normalized rate constant (1.4×10^{-2} $L\cdot hr^{-1}\cdot m^{-2}$) that is ~4-fold higher than RNIP (3.1×10^{-3} $L\cdot hr^{-1}\cdot m^{-2}$). Using limited iron (which represents their use in a DNAPL source zone with high TCE concentration), Fe/B transformed TCE into ethane (70%) and C3-C6 coupling products. The reaction displayed zero-order kinetics without deactivation. All Fe^0 in the Fe/B particles was accessible for TCE dechlorination and 92 wt. % (±0.7%) of the Fe^0 was used to reduce TCE. H_2 evolved from Fe/B with TCE presence was used to reduce TCE and adding H_2 to the reactor increased both the rate and efficiency of TCE dechlorination, indicating that a catalytic hydrodechlorination pathway exists. Termination of the reaction with sufficient H_2 remaining indicated that the catalyst may be Fe^0 or a transient Fe-(hydr)oxide phase.

<u>FeB^{cr}.</u> Annealing FeB caused the particles to become more crystalline. The reactivity of crystalline FeB^{cr} and RNIP (below) were similar and different from FeB even though FeB^{cr} has a more similar chemical composition with FeB than RNIP. H_2 was no longer activated and used to transform TCE. TCE was transformed mainly into acetylene, reducing the amount of Fe^0 needed per mol TCE degraded into half than with FeB. However, ~40% of the Fe^0 was inaccessible which counteracted this efficiency.

<u>RNIP:</u> RNIP yielded the unsaturated product acetylene under iron limited conditions and ethylene using excess iron. Reactions displayed pseudo-first-order kinetics for both cases. Acetylene was the main intermediate and indicated that β-elimination was the dominant TCE reduction pathway for RNIP. Adding H_2 did not change the reaction rate of efficiency of RNIP particles. Reaction rates, pathways, and products distribution indicate that RNIP behaves as micro-scale iron filings for TCE dechlorination.

The observed differences between FeB and RNIP/FeB^{cr} were attributed to the degree of crystallinity of the particles. The amorphous (crystallites ≤1nm) structure gave FeB the

ability to activate H_2, and resulted in saturated products (e.g. ethane). Crystallizing the Fe/B took away this ability, and resulted in the formation of unsaturated products (e.g. acetylene), incomplete use of Fe^0, and lower reactivity. The chemical composition (presence or absence of boron) plays a less important role. Crystalline nanoiron therefore behaves likes micron sized iron, and the TCE reduction reaction was faster due only to the higher surface area the smaller particles posses.

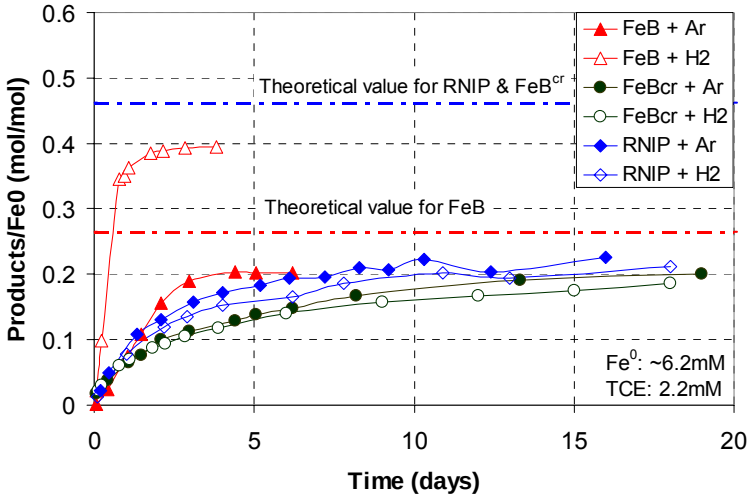

Figure 11. Total TCE products formed in reactions with FeB and FeB^{cr}.

Lifetime and reactivity of RNIP and the effect of groundwater constituents on the lifetime and reactivity of nanoiron. In the subsurface, nanoiron can be oxidized by TCE (desired) or by other competing oxidants such as H^+ which is reduced to H_2 (undesirable since RNIP cannot activate and use H_2). The reaction order of H_2 evolution with respect to Fe^0 and with respect to $[H^+]$ was determined in batch reactors to understand the geochemical factors controlling its lifetime under different pH conditions. Similarly, the reaction order of TCE dechlorination with respect to Fe^0 and with respect to $[H^+]$ was quantified in order to accurately predict the lifetime of RNIP under in situ conditions. RNIP reactivity for TCE reduction over particle lifetime at low TCE concentrations was assessed. The resulting reaction orders are summarized in Table 5 and a summary is provided below. Additional details can be found in Liu and Lowry, 2006.

Table 5. Reaction orders of H_2 evolution and TCE reduction

	Reaction order with respect to	
	Fe^0 content	**H^+ concentration**
H_2 evolution	First-order	First-order
TCE reduction	Near zero-order	Near zero-order

First order H_2 evolution with respect to Fe^0 content and $[H^+]$. A pseudo-first-order rate of H_2 evolution from RNIP having a Fe^0 content of 27 wt% at pH 8.9 was observed over a 280-day period (Figure 12a). The reaction rate constant $k_{obs,H2}$ = 3.1±1.8 ×10^{-3} day^{-1}

and the half life time ranged from 140 to 530 days. The first order reaction with respect to Fe^0, i.e. $d[H_2]/dt = k_{obs,H2}\cdot[Fe^0]$, was confirmed as the initial H_2 production rate was proportional to the initial Fe^0 content. The exponential decrease (i.e. first-order decay) of Fe^0 content over 2 years of exposure to water with $k_{obs,\ Fe0}$ = 6.0±2.1 $\times 10^{-3}$ day^{-1} further supporting the first order H_2 production with respect to Fe^0 content.

At different pH (6.5, 7.0, 7.5, 8.0, 8.5, and 8.9), the H_2 evolution from RNIP with a Fe^0 content of 9.6 wt% was pseudo-first-order with respect to the Fe^0 content. The H_2 evolution rate decreased with increasing pH between pH 6.5 to 8.0, but increases above pH=8 had no additional effect (Figure 12b). The Fe^0 was consumed (which reflects the particle lifetime) in two weeks at pH ≤7.5, but particle lifetimes were as high as 9 months at pH≥8.0. Thus, the groundwater pH will play a significant role controlling the lifetime of RNIP in the subsurface, particularly when used for plume treatment at low TCE concentration.

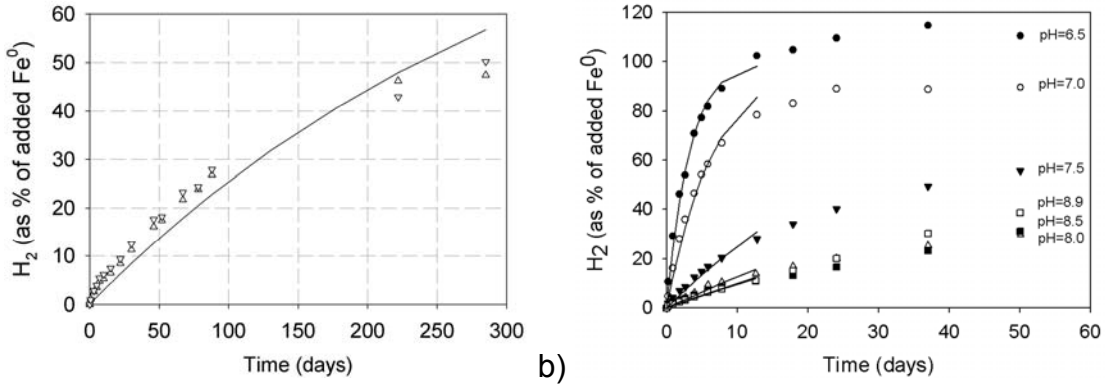

a) b)

Figure 12. a) The first order H_2 production with respect to Fe^0 content (from 500mg/L RNIP with 27% Fe^0 content; data are from duplicate reactors); b) the first order H2 production with respect to $[H^+]$ (from 300mg/L RNIP with 9.6% Fe^0 content, in the presence of 50mM HEPES to buffer solutions to desired pH).

Near zero-order TCE reaction with respect to Fe^0 content and $[H^+]$. Focusing on the long-term behavior shown in Figure 13,a, $k_{obs,TCE}$ (open symbols) did not decrease appreciably as the Fe^0 content of RNIP (filled symbols) decreased during reaction/aging in water. The moderate increase in $k_{obs,TCE}$ over the 7 month period is due to a decrease of pH in the reactor due to the reduction of TCE and formation of HCl. The relatively constant $k_{obs,TCE}$ over the life of the particles (hence a wide range of Fe^0 content, e.g. from 48% to 9.6%) suggests that the reaction with TCE is essentially zero order with respect to Fe^0 (particle age). RNIP continues to degrade TCE at a stable reaction rate constant until the Fe^0 content reaches <5%, and indicated that nearly all of the Fe^0 can be utilized.

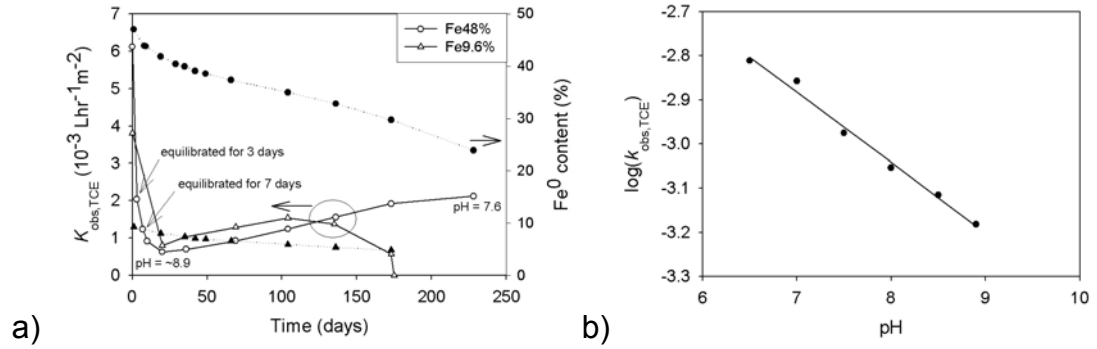

Figure 13. a) Fe^0 content (filled symbols) and surface area normalized TCE reaction rate constants ($k_{obs,\ TCE}$, $10^{-3}L \cdot hr^{-1} \cdot m^{-2}$, open symbols) over the lifetime of Fe48% and Fe9.6%. RNIP is 2g/L; b) TCE reaction rate constant $k_{obs,\ TCE}$ vs. pH.

The TCE reaction rate constant with RNIP (9.6 wt% Fe^0) content increased monotonically as the pH decreased from 8.9 to 6.5. Decreasing pH from 8.9 to 6.5 resulted in a doubling of the observed TCE reaction rate constant, which is an order of magnitude less than the increase for k_{H2} over the same pH range. A linear relationship between the logarithm of reaction rate constant and pH was obtained (Figure 13b). The slope indicates the 0.16 reaction order of TCE degradation with respect to $[H^+]$, representing a weak dependence on pH and that H^+ is not a dominant part of the rate limiting step of TCE dechlorination by RNIP (Liu and Lowry, 2006).

These studied indicate that the solution pH is the critical factor influencing the lifetime of RNIP nanoiron, e.g. RNIP loses reactivity in less than two weeks at pH 6.5 while it remains reactive for several months at pH 8.9. RNIP reactivity for TCE reduction is weakly dependent on particle age or solution pH and thus the RNIP is expected to have high reactivity as fresh particles over the lifetime. The difference between the reaction orders for H_2 evolution and TCE dechlorination with respect to Fe^0 content and $[H^+]$ can be attributed to differences in the rate controlling steps for each reaction.

Effect of groundwater constituents on the lifetime and reactivity of RNIP. Groundwater constituents, including varying TCE concentrations, individual groundwater solutes, and the solutes contained in synthetic and natural groundwater, affected TCE reduction and H_2 evolution differently. H_2 evolution was generally unaffected except in the presence of high concentrations of competing oxidants. TCE reduction was more affected, however, the (inhibitory) effect of the groundwater constituents was usually small and at most a factor of 7.

Effect on TCE concentration and groundwater solutes on H_2 evolution. The H_2 evolution rate at pH 7.0 (final pH ~7.4) was relatively unaffected by the presence of TCE compared to the absence of TCE (Figure 14). However, the total H_2 evolved was lower and stopped earlier as the TCE concentration increased. H_2 evolution stopped at 6 days, 18days, and 54days when H_2 accounted for 7%, 23%, and 40% of the Fe^0 in the

particles (assuming $Fe^0 \rightarrow Fe_3O_4$) at TCE concentrations of 8.4 mM, 1.3mM, and 0.46mM, respectively. Particle reactive lifetime was estimated ~10 days and 40 days at TCE concentrations of 8.4 mM (saturation) and 1.3mM respectively as thereafter TCE reduction was no longer observed.

H_2 evolution was not affected by the presence (5mN) of individual non-redox-reactive groundwater anion Cl^-, SO_4^{2-}, HCO_3^-, $H_2PO_4^-$, nor by the solutes in synthetic and natural groundwater water, relative to H_2 evolution in deionized water. A very high concentration (5mN) of NO_3^- completely terminated H_2 evolution in the first two days, and presumably due to the formation of a passivating layer as the pH increased to >11. These results indicate that the lifetime of RNIP should not be affected by the presence of common non-redox active groundwater solutes. Details of these studies are to appear in Liu et al., 2007.

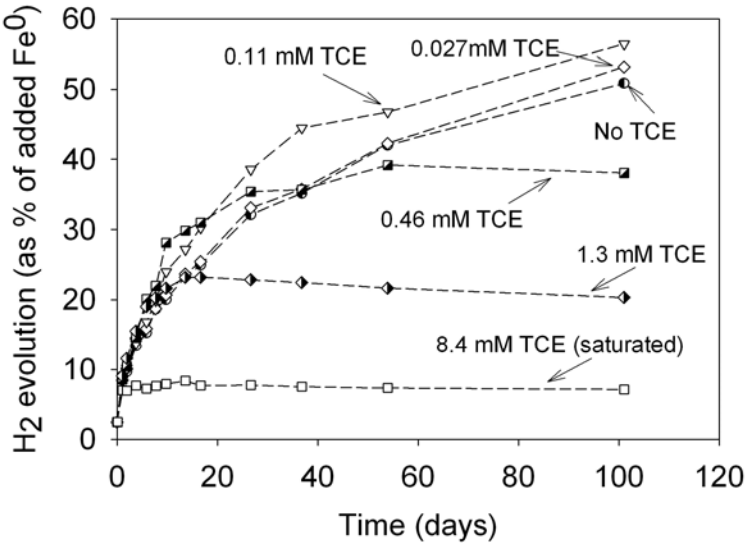

Figure 14. Effect of TCE concentrations at 670mg/L Fe48% RNIP, pH = 7.0 buffered with 50mM HEPES on H_2 evolution rates.

Effect of TCE concentration and groundwater solutes on the rate of TCE reduction. TCE reduction remained pseudo-first-order with respect to TCE over a TCE concentration range from 0.027mM to 1.3mM. The TCE reaction rate constants (k_{TCE}) decreased at higher TCE concentrations, but by less than a factor of 2 while the TCE concentration increased ~300-fold from 0.027 to 8.4mM. The stable reaction rate constant corresponds to an increased initial TCE reaction rates with increasing TCE concentration, indicating a more rapid reduction in TCE mass at the DNAPL source area (high concentration) relative to a plume (low concentration).

The presence of redox-competing oxidants such as nitrate affected TCE reduction by NZVI, but only when present at very high concentration. Nitrate present at 0.2mN and 1mN NO_3^- did not affect the TCE reduction rate despite an increase in the reactor pH to ~10. NO_3^- present at 5mM stopped the TCE reaction after only 2 days, presumably due to stimulating the formation of a passivating iron oxide layer (pH=11).

The addition of individual anions (5 mN) decreased NZVI reactivity with TCE in increasing order $Cl^- < SO_4^{2-} < HCO_3^- < HPO_4^{2-}$ (Figure 15a). The inhibition by phosphate in the form of $HPO_4^{2-}{}_{(aq)}$ on the TCE reaction was 7-fold from $5.3\times10^{-3}L\cdot hr^{-1}\cdot m^{-2}$ without solutes to $0.76\times10^{-3}L\cdot hr^{-1}\cdot m^{-2}$. The order of the effect is consistent with the affinity of anion complexation to hydrous ferric oxide (HFO) $Cl^- < SO_4^{2-} < HCO_3^- < HPO_4^{2-}$ at pH 8.9 based on their reported stability constants, and thus the blockage of the access of TCE to surface reactive sites by the anions complexation with Fe(II) and Fe(III) is likely responsible to this decline of TCE reduction rates.

The relatively minor effect of the presence of various concentration of TCE on H_2 evolution as well as the small effect of the presence of ≤1mM NO_3^- on both TCE reduction and H_2 evolution indicates that the presence of these solutes will not significantly affect the application of RNIP in the field. This was further validated using groundwater from a DoD site at Paris Island, SC. The groundwater (GW) contained commonly encountered anions, Cl^-, SO_4^{2-}, and HCO_3^- balanced by the main cations Na^+, Ca^{2+}, and Mg^{2+} (Table 6). TCE reaction rate constant in Paris Island GW was ~7 times smaller than in DI water (Figure 15b). Reaction with the synthesized groundwater (SGW) with the same inorganic composition as the GW was also adversely affected but to a smaller extent, indicating the solutes alone are not responsible for the observed decline in NZVI reactivity with TCE. It is likely that the presence of organic carbon in the groundwater (9.6 mg/L) was responsible for the additional decrease in reactivity.

Table 6. Paris Island, SC groundwater quality.

Parameter	Ca^{2+}	K^+	Mg^{2+}	Na^+	HCO_3^-	Cl^-	SO_4^{2-}	NO_3^-	pH	TOC
mM	0.89	0.04	0.45	6.09	1.18	5.32	1.23	ND [a]	6.0	
mg/L	35.5	1.48	10.8	140	72.1	189	118	ND [a]		9.6

[a] ND: non-detected, measured using ion chromatography at CEE lab at CMU.

Effect of polymer modifiers on RNIP reactivity with TCE. RNIP particles remained reactive when surface modifiers (polymer or surfactant) were added to prevent particle aggregation and improve particle transportability in groundwater system. Compared to that using bear RNIP without polymer modification, the TCE reduction was inhibited to up to a factor of 10 using RNIP modified with polymers at concentrations which provide sufficient stability for nanoiron suspension,. The inhibition by the polymer coatings depended on the polymer type. In comparison to the bare RNIP, surface modification by SDBS, tri-block copolymers with PSS-462 and with PSS-650 decreased the TCE dechlorination rate by a factor of 4 for SDBS and PSS-462, and a factor of 9 for PSS-650 (Figure 16). The decrease in the TCE dechlorination rate by the surface modifiers correlates with increasing colloidal stability, PSS-650>PSS-462~SDBS, and with the molecular weight of the modifier used. These results indicate that stabilization and reactivity must both be taken into consideration when choosing polymer/surfactant types for particle modification as increased stability comes at the price of decreased reactivity

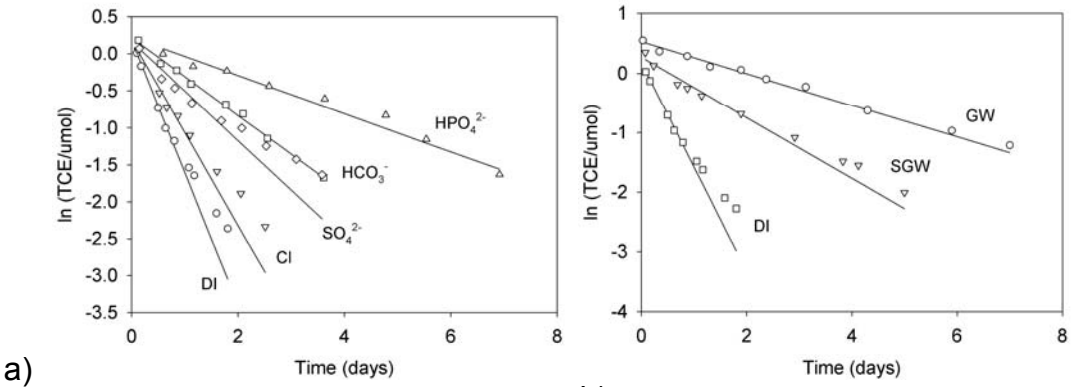

Figure 15. TCE reduction using 2g/L RNIP (without added buffer), initial C_{TCE} = 0.027mM; a) in the presence of individual 5mN non-competing anions Cl^-, SO_4^{2-}, HCO_3^-, HPO_4^{2-}; b) in synthesized groundwater and natural groundwater.

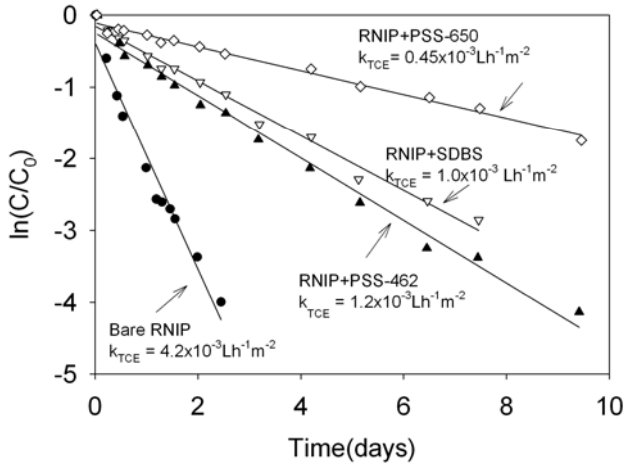

Figure 16. The effect of polymer and surfactant modification on RNIP reactivity for TCE reduction.

2.5 Particle Mobility

Transport studies were conducted in water saturated columns to better understand the geochemical factors affecting the mobility of bare and polymer-modified RNIP. Experiments were also conducted with partial DNAPL saturation to assess the ability of polymer-modified RNIP to target DNAPL in situ. Columns used AGSCO silica sand (ASTM D-1556) with an effective porosity of 0.33. RNIP modified with 1) triblock copolymers alone, 2) SDBS surfactant and 3) polyaspartate (MRNIP supplied by Toda America, Inc.) were used. To elucidate the operable filtration mechanisms, the pore scale transport behavior of the particles was observed using micro-fluidic flow cells, and direct nanoiron-silica sand grain interactions were probed by using a Quartz Crystal Microbalance (QCM) to measure nanoiron adsorption to a silica-coated substrate.

Detailed methods are described in Saleh et al. 2007 and are to appear in Saleh et al., 2007b.

Mobility of bare and modified RNIP. RNIP (bare and modified) mobility through sand-packed columns (10-cm) was evaluated at high (3g/L) particle loadings and low ionic strength (1 mM) to represent injection conditions into a contaminated sandy aquifer. The eluted mass for each of the particles is shown in Figure 17. At 3 g/L, bare RNIP was essentially immobile (1.4 $\pm$ 3% mass elution) through a 10-cm saturated sand column at low ionic strength. Retrieving the sand from the column and analyzing for iron revealed that most particles were trapped within the first 1 to 2 cm of the column. However, the mobility of bare RNIP depended on the particle concentration. At low concentration (180 mg/L) more than half of the particles eluted from the column, but elutability decreased as the particle concentration increased, and is highly inefficient (<2%) at the concentration required to make field application economical (3 g/L). At this concentration, the higher particle collision frequency makes RNIP aggregation rapid and may promote cake filtration. MRNIP, polymer- and SDBS-modified RNIP elution was greater, where the triblock copolymer and MRNIP eluted at 95% and 98%, respectively (Figure 17). SDBS was not as effective as the polymer but still improved RNIP elution to 48%. These results indicate that surface modification is essential for reasonable transport at the high particle concentrations needed to be effective for field application, even at low ionic strength.

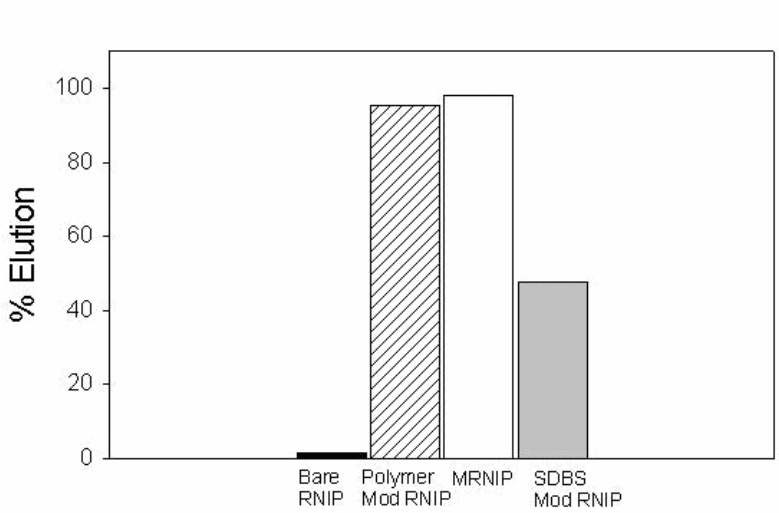

Figure 17. Particle elution and effect of modifiers.

Effect of Ionic Strength on Mobility. Coatings that improve colloidal stability primarily by increasing the surface charge of the particles (electrostatic stabilization) are susceptible to changes in the solution ionic composition and strength. Groundwater typically contains a variety of cations and anions due to dissolution of minerals or anthropogenic inputs, and groundwater ionic strengths can range from a few mM up to several hundred mM. Increasing the ionic strength of the suspension screens the surface charge of colloidal particles and thus reduces EDL repulsion. The elution data for bare and modified RNIP at different ionic strength is shown in Figure 18. Adding a monovalent 1:1

electrolyte (NaCl) to increase the ionic strength from 1 to100 mM significantly decreased the mobility of modified RNIP. SDBS-modified RNIP and MRNIP mobility decreased significantly as the ionic strength is increased. Both of the PMAA-PMMA-PSS triblock copolymer-modified RNIP particles, however, eluted (~50%) even at 100mM [Na^+]. Triblock copolymer-modified RNIP elution was superior to either MRNIP or SDBS-modified RNIP at any ionic strength examined, indicating that electrosteric repulsions afforded by large molecular weight polyelectrolytes are preferable for RNIP transport at moderate or high ionic strength. Divalent cations, such as Mg^{2+} and Ca^{2+} present in groundwater had an even greater effect as they were more efficient at compressing the EDL. An in depth investigation of the effect of concentration of monovalent and divalent cations on the mobility of the particles is addressed below.

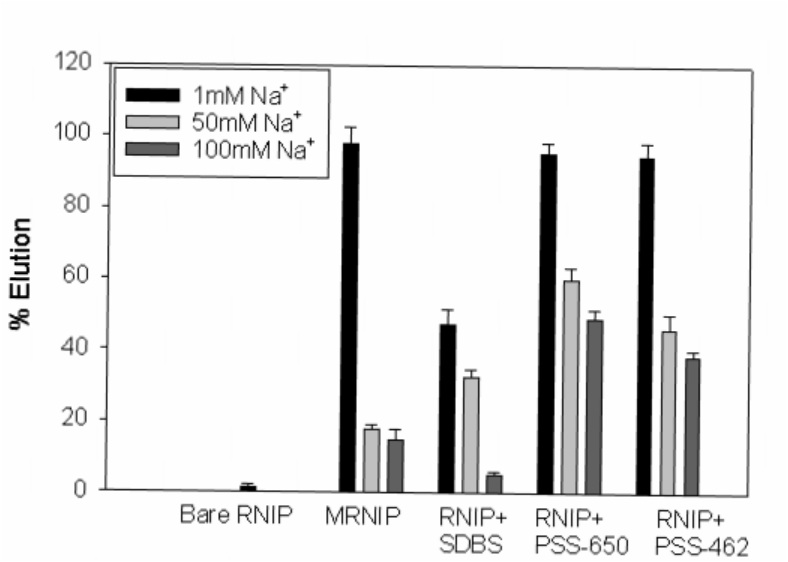

Figure 18. Effect of ionic strength (monovalent cations) on nanoiron transport

Pore-scale Understanding of the Transport/Filtration Mechanisms. To better understand the filtration mechanisms and the reasons for the enhanced transport of modified nanoiron relative to bare nanoiron, saturated sand-filled microfluidic flow cells equipped with a digital camera were used to observe RNIP filtration. A Quartz crystal microbalance (QCM), where particle adsorption to a silica surface was monitored as a function of time, was used to qualitatively determine the "stickiness" of bare and modified RNIP to quartz surfaces. Together, these techniques were able to distinguish between straining due to aggregation, and filtration due to attachment to sand grains.

Images from the micro-fluidic cell during transport of bare RNIP indicate that RNIP particles stick to the silica surface (Figure 19a). The size of primary RNIP particles is below the optical resolution of the microscope, so it is evident that RNIP aggregates were present and adhered to the sand grains. A time series of microscope images (Figure 19b-c) indicated that after the initial attachment of RNIP, RNIP subsequently attached to previously attached RNIP aggregates, rather than to bare regions of the sand surface. This implies that the particle-particle interactions for bare RNIP are stronger than for RNIP-sand grain interactions. This is consistent with the observations for RNIP aggregation and the magnitude of the magnetic attractive forces for these particles. Continued RNIP attachment eventually resulted in pore plugging (Figure 19d).

Polymer modified RNIP was also used in such flow cell experiments, and the particles did not attach to sand surfaces and pore plugging did not occur. This behavior suggests that clean bed filtration models that typically consider only particle-sand grain interactions may not be appropriate for describing nanoiron transport. Rather, filter ripening models that consider particle-particle interactions and attachment are more suitable.

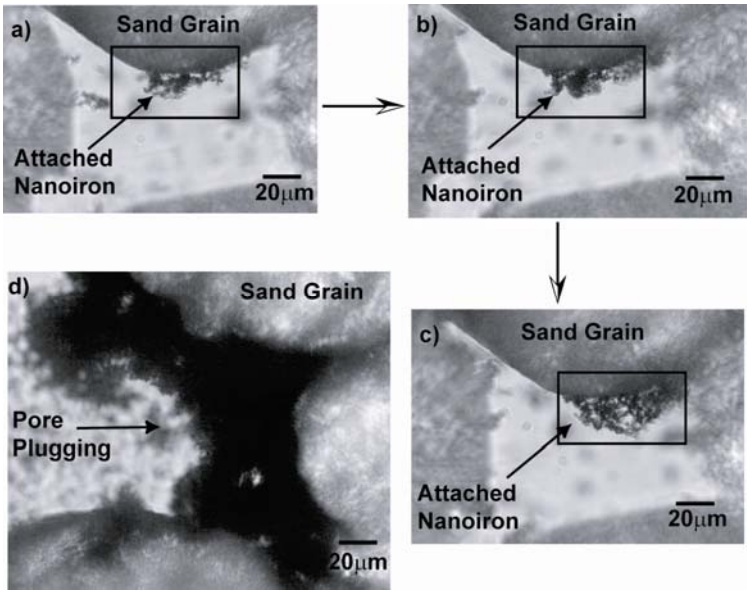

Figure 19 a-d. Micro-fluidic cell time-series images showing straining and subsequent pore-plugging of nanoiron.

The importance of particle-sand grain interactions (attachment) in predicting nanoiron mobility was further demonstrated by the QCM data for particle adhesion to a silica-coated crystal in 1 mM $NaHCO_3$ solutions (Figure 20). The downward shift in crystal resonant frequency change (indicating direct particle attachment to the silica) is significantly higher for bare RNIP than for either MRNIP, PMAA-PMMA-PSS polymer-modified RNIP, or SDBS-modified RNIP. Thus the sticking coefficient and attachment efficiency of bare RNIP should be higher than for the other particles, which is consistent with the elution data and microfluidic cell data. The relative affinity for silica surfaces as determined by QCM (polymer-RNIP < MRNIP < SDBS-RNIP << bare RNIP) correlated well with the transport results and demonstrates that particle-collector grain attachment is important but effectively eliminated by electrosterically stabilizing RNIP with the polymer.

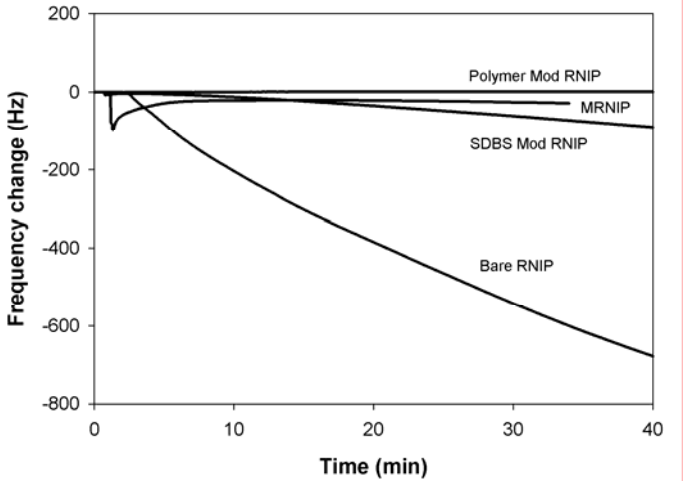

Figure 20. QCM frequency shift curves demonstrating effect of modifiers on nanoiron adsorption to silica.

Effect of modifiers on transport for varying mono and di-valent cations. To investigate the effects of varying ionic strength, transport experiments were conducted in a 60 cm long column and pore water velocity of 28 m/day. Low particle concentrations (30 mg/L) were used to better understand the effect of ionic strength and composition on particle attachment. A pulse of particles was injected into the column at varying Na^+ and Ca^{2+} concentration, followed by flush water with the same ionic strength and composition. Particles were constantly sonicated until injecting to the column to keep them dispersed. Surface modifiers evaluated were triblock copolymers, SDBS, and polyaspartate (MRNIP supplied by Toda America, Inc.). Breakthrough data were colleted and subsequently analyzed using a single collector efficiency model. Details of the experiments and results are to appear in Saleh et al., 2007b). A typical breakthrough curve is shown in Figure 21a-b. Increasing the ionic strength decreased particle elution as expected, and the effect is greater for Ca^{2+} than for Na^+ as expected. The triblock copolymer modified RNIP had breakthrough at [Na^+] as high as 1M and [Ca^{2+}] as high as 100mM. A single collector efficiency model was applied to the breakthrough data and sticking coefficients were calculated in order to compare the resistance of each modifier to changes in ionic strength. Figure 22a-c shows the data and fitted curves for different mono and di-valent cation concentration.

These curves show two critical parameters for assessing the mobility of the modified particles; the critical deposition concentration (maximum salt concentration at which sticking coefficient will reach unity) and the slope of the curve which indicates the sensitivity of the particles to increases in salt concentration. The triblock copolymer modified RNIP is the most effective modifier for transport having the highest CDC values for both Na^+ and Ca^{2+}. Polyaspartate, which is a lower molecular weight polymer, was the next best modifier followed by SDBS surfactant, consistent with the elutability studies.

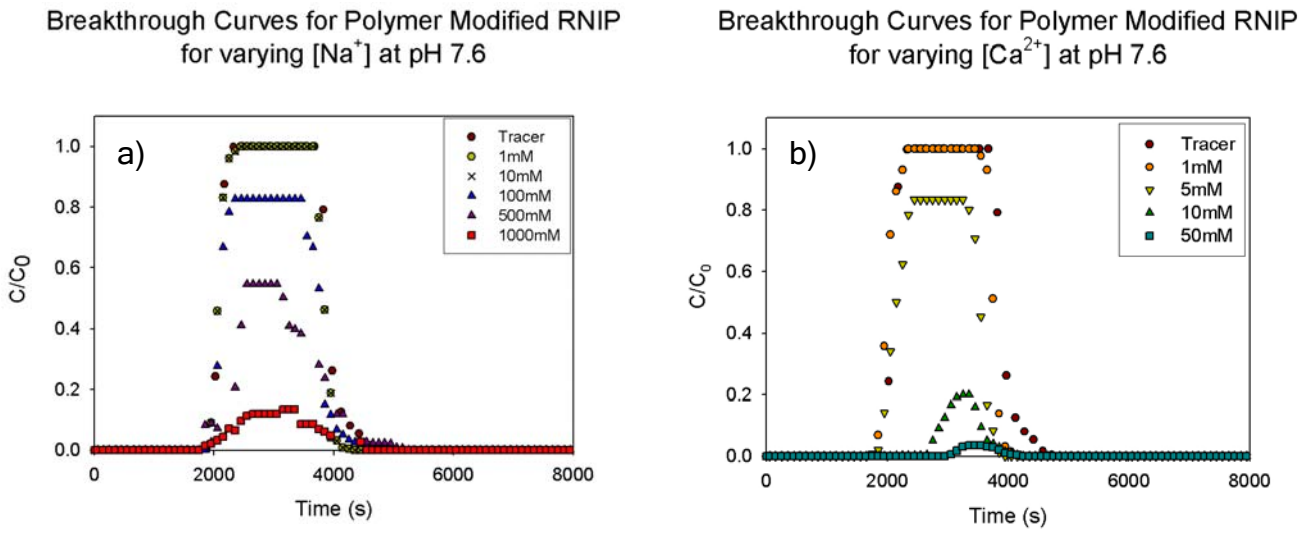

Figure 21a-b. Breakthrough curves for triblock copolymer-modified RNIP in the presence of varying concentrations of Na^+ and Ca^{2+}.

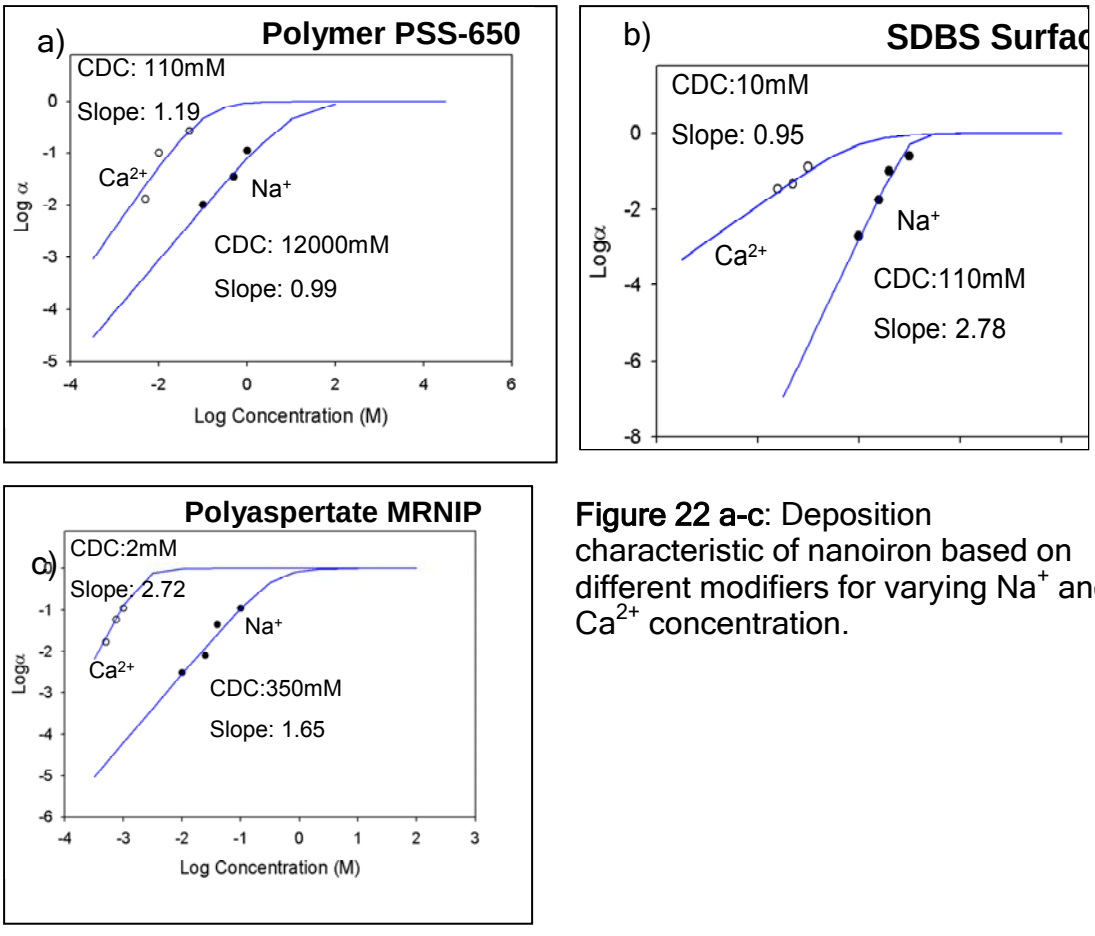

Figure 22 a-c: Deposition characteristic of nanoiron based on different modifiers for varying Na^+ and Ca^{2+} concentration.

2.6 Developing numerical models to predict transport.

The diffusion rates of nanoscale particles, particularly in inhomogeneous environments such as water/DNAPL interfaces, are sensitive to the microscopic particle structure. Their structure is challenging to fully characterize experimentally, so computer simulations on molecular length-scales (Brownian Dynamics (BD) simulations) were conducted to describe the dynamics and structure of polymer-grafted metal nanoparticles. These simulations will provide parametric inputs for macroscale simulations of particle transport in porous media.

Modeling a nanoparticle. Simulating the Brownian Dynamics of a solid nanoparticle in a solvent was somewhat more challenging than simply reproducing the known translational diffusivity of solid particles, since we aimed to correctly describe the dynamics of polymers grafted to the particle. As a result, the description of the solid particle must reproduce the correct translational and rotational diffusivities. Furthermore, the rigid nature of the particle must be included in the simulation. These tasks were accomplished by performing BD simulations of a set of nodes distributed on the surface of the nanoparticle subject to distance constraints (Ryckaert et al, 1977; Ciccotti et al., 1982; Liu, 1989; Doyle et al., 1997).

BD simulations of bare particles incorporating hydrodynamic interactions. We defined the diffusion tensor in terms of a modified form of the Rotne-Prager-Yamakawa formulation (Rotne and Prager, 1969; de la Torre and Bloomfield, 1977). Correlated random numbers were obtained by performing a Chebyshev series expansion of the square root of the diffusion tensor as described by Fixman (Fixman, 1986) and implemented by others (Kroger et al, 2000; Jendrejack et al, 2000). We tested the translational and rotational diffusions of a bare particle and compared them to theoretical predictions, as Figure 23 shows. The bead radius affected the diffusion properties of the particle. As the number of beads was increased, and the bead radius was decreased, the predicted hydrodynamic radius approached the theoretical limit. Moreover, we found that we could account for the bead radius effect on the diffusion by a simple formula, enabling us to tailor the design such that the simulation gave the correct hydrodynamic radius for the bare particle.

BD simulations of stabilized nanoparticles. Since we are looking for a representation of a stabilized particle with a limited number of beads, there must be then a balance between the number of beads representing the particle and polymer bead size. If the number of particle beads was small, we had to compensate by making the polymer beads larger in size to be able to occupy space, and thus be able to extend outwards. We tested the model against data for the hydrodynamic radius of a polystyrene-stabilized silica particle from Savin et al. (Savin et al, 2002) as Figure 24 shows. As expected, compensation in terms of polymer bead size was necessary in order to have an agreement with experimental data. Similar simulations were carried out using different number of particle beads. The information obtained from those simulations was used to model systems with various grafting densities.

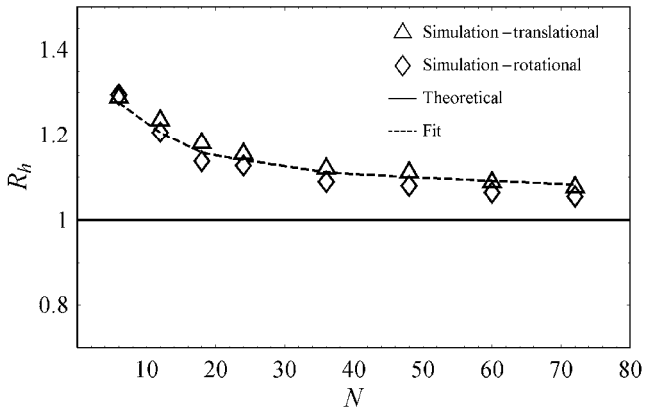

Figure 23. Hydrodynamic radius (R_h) vs. number of beads (N) representing the bare particle. The triangles are results from calculation of R_h using translational diffusion, while the diamond-shaped symbols are obtained from rotational diffusion calculations. The radius of the bare particle is unity, while the radius of the beads on the particle surface decreases with the increase of the number of beads.

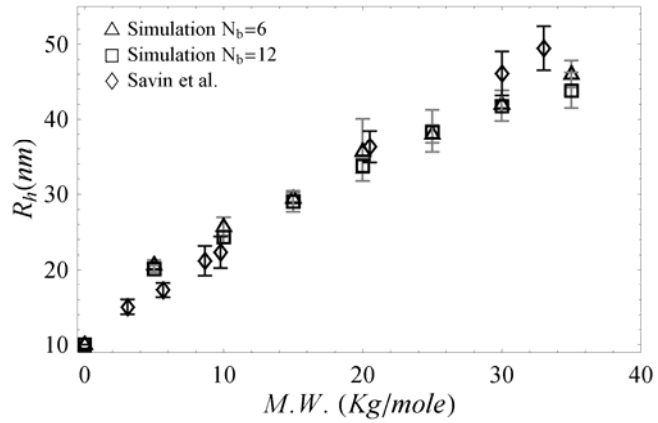

Figure 24. Hydrodynamic radius (R_h) vs. molecular weight of grafted polystyrene chains. N_b denotes the number of beads that represent the bare particle.

Modeling the hydrophile and the hydrophobe. Both of the hydrophile and the hydrophobe portions of the block copolymer were modeled as a polymer chain that has a different structure in good and poor solvent environments. We model water as being a medium that is a good solvent for polystyrene sulfonate (PSS), and a poor solvent for PMMA. On the other hand, we modeled TCE as a medium that is a good solvent for PMMA and a poor solvent for PSS. Modeling a good solvent was carried out using a "soft" exponential potential function, while modeling a poor solvent condition was carried out using Morse potential.

Modeling the polyelectrolyte. For the block copolymer components, the hydrophilic portion (PSS) is a polyelectrolyte. Thus, we used a special description for the

electrostatic forces. We used the Debye Huckel model to describe those forces, as was also done in other simulation studies (Ullner, 2003; Hayashi et al, 2003). In addition, we employed Trizac prescription (Trizac et al, 2003; Alexander et al., 1984) for charge renormalization to calculate the charge per bead (here a bead represents a given number of monomer units).

Modeling the liquid-liquid interface. The interface was modeled because both mediums (water and TCE) were implicitly modeled in Brownian Dynamics simulations. The large scale of the nanoparticle and the polymer chains in relation to a solvent molecule prohibited the modeling of such molecules directly in our situation. We started from an approach introduced by Dickinson and coworkers (Wijmans and Dickinson, 1999; Pugnaloni et al., 2003; Pugnaloni et al, 2004) to describe proteins in the presence of an interface, and modified their approach to allow for a more detailed description of a block copolymer at an interface. The potential that described the interface was tailored to describe the preferred environment of both homopolymers.

Modeling the stabilized particle in the presence of an oil-water interface. Results were obtained for a stabilized particles in the presence of an oil-water interface. A particle with a radius of 10 nm was stabilized by a block copolymer: $PMMA_{150}$-PSS_{150}. The grafting density that was chosen here was 12 polymer chains per particle. The interface is at the plane at $z = 0.0$. The water domain is at $z<0$, while the oil domain is at $z>0$. Periodic boundary conditions were employed. We assumed that the water had a salt concentration of 1mM. Figure 25 shows the movement of the particle in the oil-water domain. While the movement in the x and y directions was random, the particle was pinned slightly below the interface at the water region, indicating that particles modified with this polymer should have a thermodynamic affinity for the oil/water interface as was observed for particles modified with polymers of a similar architecture. Measurements of the polymer structure and the translational diffusivity of the composite particle provided information that can be closely related to the experimental data available from light scattering in future studies.

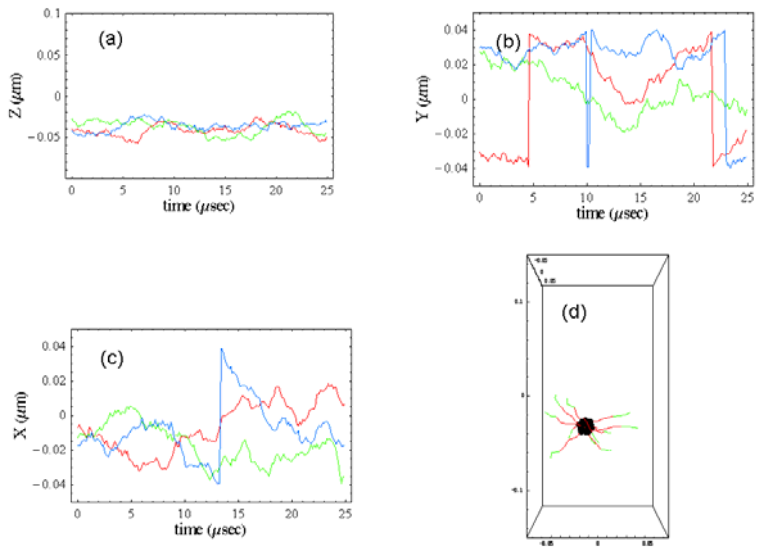

Figure 25. Results for a stabilized particle in the presence of oil-water interface. Parts (a)-(c) show the z, y and x co-ordinates of different trajectories of the center of mass of the particle (shown in different colors) with respect to time. Part (d) shows a snapshot of the particle. The red color in part (d) represents PMMA, while the green color represents PSS.

3.0 References

Alexander, S.; Chaikin, P. M.; Grant, P.; Morales, G. J.; Pincus, P. Journal of Chemical Physics 1984, 80, 5776.

Ciccotti, G.; Ferrario, M.; Ryckaert, J.-P. Molecular Physics 1982, 47, 1253-1264.

Doyle, P. S.; Shaqfeh, E. S. G.; Gast, A. P. Journal of Fluid Mechanics 1997, 334, 251-291.

Fixman, M. Macromolecules 1986, 19, 1204-1207.

Hayashi, Y.; Ullner, M.; Linse, P. J. Phys. Chem. B. 2003, 107, 8198.

Jendrejack, R. M.; Graham, M. D.; de Pablo, J. J. Journal of Chemical Physics 2000, 113, 2894-2900.

Kroger, M.; A., A.-P.; Laso, M.; Ottinger, H. C. Journal of Chemical Physics 2000, 113, 4767-4773.

Liu, T. W. Journal of Chemical Physics 1989, 90, 5826-5842.

Liu Y., Majetich, S. A., Tilton, R. D., Sholl, D. S., Lowry, G.V., (2005a). "TCE Dechlorination Rates, Pathways, and Efficiency of Nanoscale Iron Particles with Different Properties", Environ. Sci. &Technol. 39(5) 1338-1345.

Liu, Y., Choi C., Dionysiou, D., Lowry, G. V. "TCE Hydrodechlorination by Amorphous Monometallic Nanoiron." 2005. *Chem. Mat.* 17, 5315-5322.

Liu, Y., Lowry, G.V. "Effect of Particle Age (Fe^0 content) and Solution pH on NZVI Reactivity: H_2 Evolution and TCE Dechlorination". *Environ. Sci. Technol.*, 2006 40 (19) 6085-6090.

Matyjaszewski, K.; Wang, J. S., US 5,763,548, 1995.

Nurmi, J. T.; Tratnyek, P. G.; Sarathy, V.; Baer, D. R.; Amonette, J. E.; Pecher, K.; Wang, C.; Linehan, J. C.; Matson, D. W.; Penn, R. L.; Driessen, M. D. Environ. Sci. Technol. 2005, 39, 1221-1230.

Patten, T. E.; Xia, J.; Abernathy, T.; Matyjaszewski, K. Science 1996, 272, 866.

Phenrat, T., Saleh, N., Sirk, K., Tilton, R., Lowry, G. V. "Aggregation and Sedimentation of Aqueous Nanoiron Dispersions" Environ. Sci. Technol., (in press).

Ponder, S. M.; Darab, J. G.; Bucher, J.; Caulder, D.; Craig, I.; Davis, L.; Edelstein, N.; Lukens, W.; Nitsche, H.; Rao, L.; Shuh, D. K.; Mallouk, T. E. Chem. Mater. 2001, 13.

Pugnaloni, L. A.; Ettelai, R., and ; Dickinson, E. Langmuir 2003, 19, 1923.

Pugnaloni, L. A.; Dickinson, E.; Ettelai, R.; Mackie, A. R.; Wilde, P. J. Advances in Colloid and Interface Science 2004, 107, 27

Pyun, J.; Matyjaszewski, K. Chem. Mater. 2001, 13, 3436.

Rotne, J.; Prager, S. Journal of Chemical Physics 1969, 50, 4831.

Ryckaert, J.-P.; Ciccotti, G.; Berendsen, H. J. C. Journal of Computational Physics 1977, 23, 327-341.

Saleh, N., Traian Sarbu, Kevin Sirk, Gregory V. Lowry, Krzysztof Matyjaszewski and Robert D. Tilton (2005). Oil-in-Water Emulsions Stabilized by Polyelectrolyte-Grafted Nanoparticles. *Langmuir* 21, 9873-9878

Saleh, N., Phenrat, T., Sirk, K., Dufour, B., Ok, J., Sarbu, T., Matyjaszewski, K., Tilton, R., Lowry, G. V. "Adsorbed Triblock Copolymers Deliver Reactive Iron Nanoparticles to the Oil/Water Interface." 2005. *Nano Lett.* 5 (12) 2489-2494.pdf

Saleh, N., Sirk, K., Liu, Y., Phenrat, T., Dufour, B., Matyjaszewski, K., Tilton, R., Lowry, G. V. "Surface Modifications Enhance Nanoiron Transport and DNAPL Targeting in Saturated Porous Media." *Environ. Eng. Sci.* 2007, 24 (1) 45-57..

Savin, D. A.; Pyun, J.; Patterson, G. D.; Kowalewski, T.; Matyjaszewski, K. Journal of Polymer Science: Part B: Polymer Physics 2002, 40, 2667-2676.
de la Torre, J. G.; Bloomfield, V. A. Biopolymers 1977, 16, 1747-1763.
Tran, Y., P. Auroy, J. Am. Chem. Soc. 2001, 123, 3644.
Trizac, E.; Bocquet, L.; Aubouy, M.; von Grunberg, H. H. Langmuir 2003, 19, 4027.
Ullner, M. J. Phys. Chem. 2003, 107, 8097.
Wang, J. S.; Matyjaszewski, K. J. Am. Chem. Soc. 1995, 117, 5614.
Wijmans, C. M. a.; Dickinson, E. Physical chemistry and chemical physics 1999, 1, 2141.
Wijmans, C. M. a.; Dickinson, E. Langmuir 1999, 15, 8344.
Zhang, Wei-xian, J. Nanoparticle Research, 2003, 5(3-4), 323-332.

4.0 Peer Reviewed Publications

1. Sarbu, T., Koon-Yee Lin, John Ell, Daniel J. Siegwart, James Spanswick, and Krzysztof Matyjaszewski (**2004**). "Polystyrene with Designed Molecular Weight Distribution by Atom Transfer Radical Coupling." *Macromolecules* 37, 3120-3127.
2. Abdulwahab Almusallam and David S. Sholl. (**2004**) "Brownian Dynamics Study of Polymer Stabilized Particles, *Nanotechnology* 16 (7) S409-S415.
3. Liu Y., Majetich, S. A., Tilton, R. D., Sholl, D. S., Lowry, G.V., (**2005a**). "TCE Dechlorination Rates, Pathways, and Efficiency of Nanoscale Iron Particles with Different Properties", *Environ. Sci. &Technol.* 39(5) 1338-1345.
4. Saleh, N., Traian Sarbu, Kevin Sirk, Gregory V. Lowry, Krzysztof Matyjaszewski and Robert D. Tilton (**2005a**). "Oil-in-Water Emulsions Stabilized by Polyelectrolyte-Grafted Nanoparticles." *Langmuir* 21, 9873-9878.
5. Liu, Y., Hyeok Choi, Dionysios Dionysiou, Gregory V. Lowry (**2005b**). TCE Hydrodechlorination by amorphous monometallic nanoiron." *Chem Mat.* 17, 5315-5322.
6. Saleh, N., Phenrat, T., Sirk, K., Dufour, B., Ok, J., Sarbu, T., Matyjaszewski, K., Tilton, R., Lowry, G. V. **(2005b)**. "Adsorbed Triblock Copolymers Deliver Reactive Iron Nanoparticles to the Oil/Water Interface." *Nano Lett.* 5 (12) 2489-2494.
7. Saleh, N., Sirk, K., Liu, Y., Phenrat, T., Dufour, B., Matyjaszewski, K., Tilton, R., Lowry, G. V. **(2006)** "Surface Modifications Enhance Nanoiron Transport and DNAPL Targeting in Saturated Porous Media." *Environ. Eng. Sci.* 24 (1) 2007 p.45-57.
8. Liu, Y., Lowry, G.V. **(2006)** "Effect of Particle Age (Fe0 content) and Solution pH on NZVI Reactivity: H2 Evolution and TCE Dechlorination". *Environ. Sci. Technol.*, *Environ. Sci. & Technol.* 40(19), 6085.
9. Phenrat, T., Saleh, N., Sirk, K., Tilton, R., Lowry, G. V. **(2006)**. "Aggregation and Sedimentation of Aqueous Nanoiron Dispersions" *Environ. Sci. Technol.*, (in press).
10. Liu, Y., Phenrat, T., Lowry, G. Effect of groundwater constituents on H_2 evolution and TCE reduction by NZVI. (in preparation for *Environ. Sci. Technol.*).
11. Saleh, N., Matyjaszewski, K., Tilton, R., Lowry, G. V. Ionic Strength and Counter-ions affect the mobility of surface-modified NZVI in water-saturated sand columns. (in preparation for *Environ. Sci. Technol.*).
12. Phenrat, T. et al. Effect of surface modification on aggregation and sedimentation of aqueous nanoiron dispersions (in preparation for *J. Nanopart. Res.*).
13. Abdulwahab S. Almusallam and David S. Sholl. Brownian Dynamics simulations of copolymer-stabilized nanoparticles in the presence of an oil-water interface (in preparation for *Langmuir*).
14. Sirk, K., Saleh, N., Phenrat, T., Lowry, G., Matyjaszewski, K., Tilton, R. Adsorption of triblock copolymers to nanoscale zerovalent iron. (in preparation for Env. Eng. Sci.).
15. Phenrat, T., Saleh, N., Sirk, K., Tilton, R., Lowry, G. Effect of Surface modification on NZVI reactivity with TCE. (In preparation for Environ. Sci. Technol.).

5.0 Presentations/Conference Proceedings

16. Lowry, G., Redden, G., Tilton, R., Sholl, D., Majetich, S., Matyjaszewski, K., Meakin, P., Rollins, H., "Transport, Targeting, and Applications of Metallic Functional Nanoparticles for Degradation of DNAPL Chlorinated Organic solvents". Presented at the DOE Environmental Management Science Program FY2003 Annual Meeting, Pasco, WA, May 7, 2003.
17. Liu, Y., Lowry, G., Majetich, S., "TCE Dechlorination by Iron Nanoparticles: Effect of the Surface Oxide Layer Growth on the TCE Dechlorination Rate", Presented at the American Chemical Society 35th Central Regional Meeting. Pittsburgh, PA October 19-22.
18. Lowry, G., Liu, Y., Majetich, S., "Factors Affecting the Reactivity, Efficiency, and Lifetime of Iron Nanoparticles for In Situ Degradation of TCE". Presented at the American Geophysical Union Fall Meeting 2003, San Francisco, CA, December 8-12, 2003.
19. Lowry, G., Redden, G., Tilton, R., Sholl, D., Majetich, S., Matyjaszewski, K., Meakin, P., Rollins, H., "Transport, Targeting, and Applications of Metallic Functional Nanoparticles for Degradation of DNAPL Chlorinated Organic solvents". In the proceedings of the 227th American Chemical Society National Meeting, March 31, 2004. Vol. 44(1), p. 488.
20. Lowry, G., Tilton, R., Sholl, D., Majetich, S., Matyjaszewski, K., "Developing Functional Fe^0-based Nanoparticles for In Situ Degradation of DNAPL Chlorinated Organic Solvents", Presented at the 227th American Chemical Society National Meeting, April 1, 2004, Anaheim, CA.
21. Lowry, G., "Nanomaterials: Novel Applications for DNAPL and PCB Impacted Sites". Presented at the April meeting of the Three Rivers Chapter of the Academy of Certified Hazardous Materials Managers, Pittsburgh, PA. April 8, 2004.
22. Tilton, Robert, Sirk, K., Saleh, N., Lowry, G., "Development of Polymer-Decorated Nanoparticles for Targeted Delivery of Remediation Agents to the Trichloroethylene/Water Interface", 78th ACS Colloid and Surface Science Symposium, New Haven, CT. June 20-23, 2004.
23. Liu, Y., Lowry, G.V., "Comparative evaluation of the reactivity and efficiency of two types of nanoscale zero-valent iron for reductive dehalogenation of TCE DNAPL". In the Proceedings of the Environmental Chemistry Division, 228th American Chemical Society National Meeting, Philadelphia, PA, Aug 22-26. Vol. 45(1).
24. K. Sirk, N.B. Saleh, Y. Liu, T. Sarbu, A.S. Almusallam, G. Lowry, K. Matyjaszewski, S. Majetich, D. Sholl, R. Tilton, "Development of Polymer-Modified Nanoparticles for Targeted Delivery of Remediation Agents to DNAPL/Water Interfaces", AICHE 2004 National Meeting, November 7-12, 2004, Austin, TX.
25. Almusallam, A. and Sholl, D., "Brownian dynamics study of polymer-stabilized nanoparticles". Presented at the Midwest Thermodynamics and Statistical Mechanics Conference, June 4, 2004, Buffalo, New York.
26. Yueqiang Liu, S.A. Majetich, R.D. Tilton, D.S. Sholl, and G.V. Lowry, "Aqueous-phase TCE Dechlorination by Nanoscale Fe^0 Particles: Effect of Iron Properties

on Reaction Pathways and Products Formed." Presented at the 42nd Annual Pittsburgh-Cleveland Catalysis Society Meeting, Pittsburgh, PA, June 18, 2004.
27. Lowry, G., Liu, Y., Tilton, R., Sholl, D., Sirk, K., Saleh, N., Sarbu, T., Majetich, S., Matyjaszewski, K., "Developing Functional Fe0-based Nanoparticles for In Situ Degradation of DNAPL Chlorinated Organic Solvents", Presented at the U.S. EPA 2004 Nanotechnology Science to Achieve Results (STAR) Progress Review Workshop - Nanotechnology and the Environment II. August 18-20, 2004.
28. Saleh, N. B., Sirk, K., Sarbu, T., Tilton, R.D., Matyjaszewski, K., Lowry, G. V. (2005). Transport and DNAPL Targeting of Polyelectrolyte- and Surfactant-modified Nanoiron. In the Proceedings of the Environmental Chemistry Division, 230h American Chemical Society National Meeting, Washington, DC August 28-September 1.
29. Yueqiang Liu, Hyeok Choi, Dionysios Dionysiou, and Greg Lowry (2005). Particle-scale understanding of TCE hydrodechlorination in water by poorly ordered nanoiron. In the Proceedings of the Environmental Chemistry Division, 230h American Chemical Society National Meeting, Washington, DC August 28-September 1.
30. Saleh, N. B., Sirk, K., Sarbu, T., Lowry, G. V., Tilton, R.D., Matyjaszewski, K., Redden, G. (2005). Targeted Delivery of Nanoiron to the NAPL-water Interface. 79th ACS COLLOID AND SURFACE SCIENCE SYMPOSIUM, Clarkson University, Potsdam, NY. June 12-15.
31. Sirk, K., Saleh, N. B., Matyjaszewski, K., Lowry, G. V. Tilton, R.D. Development of Triblock Copolymers as Dispersants and Interfacial Delivery Vehicles for Reactive Nanoparticulate Iron. AICHE Annual Meeting, Engineering Sciences and Fundamentals Division, Cincinnati, OH. October 30-Novermber 4, 2005.
32. Lowry, G. V. (2005). "Delivering Polymer-modified Fe0 Nanoparticles to Subsurface Chlorinated Organic Solvent DNAPL." US EPA Nanotechnology and the Environment: Applications and Implications Progress Review Workshop III, Washington D.C., October 26-28, 2005.
33. Lowry, G.V., T. Phenrat, N. Saleh, Y. Liu, K. Sirk, R. Tilton (2005). Creating Stable Nanoiron Suspensions for Efficient Subsurface Delivery to DNAPL Source Zones. SERDP Partners in Environmental Technology Technical Symposium & Workshop, Washington, D.C. November 28-30, 2005.
34. Robert D. Tilton, Gregory V. Lowry, Krzysztof Matyjaszewski, Navid B. Saleh, Kevin Sirk, Yueqiang Liu, Traian Sarbu, Bruno Dufour, Jeongbin Ok, Tanapon Phenrat, and Hye-Jin Kim. (2006). "Triblock copolymers as nanoparticulate iron targeted delivery vehicles for source-zone remediation of contaminated aquifers." Division of Colloid and Surface Chemistry, 231st ACS National Meeting, Atlanta, GA, March 26-30, 2006.
35. Lowry, G. V., Saleh, N., Sirk, K., Phenrat,T., Dufour, B., Matyjaszewski, K., Tilton, R.D. (2006). "Triblock copolymer coatings enhances nanoiron transport and localizes nanoiron at the DNAPL/water interface". Division of Geochemistry, 231st ACS National Meeting, Atlanta, GA, March 26-30, 2006.
36. Lowry, G. V., Saleh, N., Sirk, K., Phenrat,T., Dufour, B., Matyjaszewski, K., Tilton, R.D. (2006). "Effect of Groundwater Geochemistry on Nanoiron Transport in

Saturated Porous Media". In the Proceedings of the Environmental Chemistry Division, 231st ACS National Meeting, Atlanta, GA, March 26-30, 2006.
37. Lowry, G., Liu, Y. (2006). "Effect of pH and Aging on NZVI Corrosion Rate and Reactivity with TCE." In the Proceedings of the Environmental Chemistry Division, 231st ACS National Meeting, Atlanta, GA, March 26-30, 2006.
38. Gregory V. Lowry, N. Saleh, Y. Liu, T. Phenrat, K. Sirk, B. Dufour, T. Sarbu, K. Matyjaszewski, R. Tilton. (2006). "Nanoiron Treatment of DNAPL Source Zones: Efficient Delivery and DNAPL Targeting." The Fifth International Conference on Remediation of Chlorinated and Recalcitrant Compounds, Monterey, CA. May 22-25, 2006.
39. Saleh, N., Matyjaszewski, K., Tilton, R.D., Lowry, G. V. (2006). "Long-range Transport of Polymer-modified Nanoiron in Saturated Porous Sand and Real Aquifer Media." 80th ACS Colloid and Surface Science Symposium, Boulder, Colorado June 18-21.
40. Kevin Sirk, Navid Saleh, Hye-Jin Kim, Tanapon Phenrat, Traian Sarbu, Bruno Dufour, Jeongbin Ok, Krzysztof Matyjaszewski, Gregory V. Lowry and Robert D. Tilton. (2006). "Nanoiron surface modification by amphiphilic triblock copolymers for enhanced stability, transportability and accumulation at the NAPL/water interface." 80th ACS Colloid and Surface Science Symposium, Boulder, Colorado June 18-21.
41. Navid Saleh, Kevin Sirk, Tanapon Phenrat, Yueqiang Liu, Bruno Dufour, Krzysztof Matyjaszewski, Robert D. Tilton, Gregory V. Lowry (2006). "Surface modifications enhance colloidal iron transport and deliver them to the NAPL/water interface." Division of Colloid and Surface Chemistry for the 232nd ACS National Meeting, San Francisco, CA, September 10-14, 2006.
42. Lowry, G. V., Liu, Y. (2006). "Nanoiron: Reactant or Catalyst?" In the Proceedings of the Division of Environmental Chemistry for the 232nd ACS National Meeting, San Francisco, CA, September 10-14, 2006.
43. Lowry, G.V., Saleh, N., Phenrat, T., Liu, Y., Kim, H., Sirk, K., Matyjaszewski, K., Tilton, R. (2006). "Delivering Polymer-modified Fe0 Nanoparticles to Subsurface Chlorinated Organic Solvent DNAPL." US EPA Nanotechnology and the Environment: Applications and Implications Progress Review Workshop III, Washington D.C., November 8-9, 2006.
44. Lowry, G.V., Navid Saleh, Tanapon Phenrat, Hye-jin Kim, Kevin Sirk, Robert D. Tilton, Tissa Illangasekare (2006). "Effects of Polymeric Surface Coatings on NZVI Mobility in Saturated Porous Media and Reactivity with TCE." Partners in Environmental Technology Technical Symposium & Workshop, Washington, D.C. November 28-30, 2006.
45. Lowry, G. and Liu, Y. (2006) "Lifetime and Reactivity of NZVI in Groundwater". Partners in Environmental Technology Technical Symposium & Workshop, Washington, D.C. November 28-30, 2006.
46. Lowry, G. V. (2006). "Mobility and Reactivity of Modified NZVI for In Situ Remediation of Subsurface DNAPL. International Symposium on Environmental Implications and Applications of Nano-sized Materials, National Chung Hsing University,Taichung, Taiwan. December 14, 2006.

6.0 Other Publications/Notoriety

1. "Tiny engineered particles could one day remove common pollutant", by Byron Spice, science and technology writer for *Pittsburgh Post Gazette*, feature article in science and technology section of post Gazette, 4/1/04. (http://www.post-gazette.com/pg/04092/294409.stm).
2. "Nanoparticles seek out solvents in groundwater", by Liz Kalaugher, editor NanotechWeb.org, feature article in *Nanotechweb.org* on 4/13/04 (http://nanotechweb.org/articles/news/3/4/8/1).
3. "Nanotechnology Increases Efficiency of Environmental Technologies." Article published in *Groundwater Monitoring and Remediation*, Summer 2004.
4. "Small Science may Clean a Big Problem, appeared in *The Christian Science Monitor*, Boston-Thursday February 10, 2005.
5. Special Treatment: Tiny technology tackles mega messes. Science News, Vol. 67, April 23, 2005.